

## 4.21 Earthquake Hazard Mitigation: New Directions and Opportunities

R. M. Allen, University of California Berkeley, Berkeley, CA, USA

© 2007 Elsevier B.V. All rights reserved.

4.21.1	<b>Introduction</b>	607
4.21.2	<b>Recognizing and Quantifying the Problem</b>	608
4.21.2.1	Forecasting Earthquakes at Different Spatial and Temporal Scales	608
4.21.2.2	Global Seismic Hazard	609
4.21.2.3	Changing Seismic Risk	611
4.21.2.3.1	Earthquake fatalities since 1900	611
4.21.2.3.2	Concentrations of risk	613
4.21.2.4	<b>Local Hazard and Risk: The San Francisco Bay Area</b>	614
4.21.2.4.1	The San Francisco Bay Area	614
4.21.2.4.2	Earthquake probabilities	616
4.21.2.4.3	Future losses	616
4.21.3	<b>The ‘Holy Grail’ of Seismology: Earthquake Prediction</b>	618
4.21.4	<b>Long-Term Mitigation: Earthquake-Resistant Buildings</b>	619
4.21.4.1	<b>Earthquake-Resistant Design</b>	620
4.21.4.1.1	Lateral forces	620
4.21.4.1.2	Strong-motion observations	620
4.21.4.1.3	Strong-motion simulations	621
4.21.4.1.4	New seismic resistant designs	623
4.21.4.2	<b>The Implementation Gap</b>	624
4.21.4.2.1	The rich and the poor	624
4.21.4.2.2	The new and the old	625
4.21.5	<b>Short-Term Mitigation: Real-Time Earthquake Information</b>	626
4.21.5.1	<b>Ground Shaking Maps: ShakeMap and Beyond</b>	627
4.21.5.1.1	ShakeMap	627
4.21.5.1.2	Rapid finite source modeling	628
4.21.5.1.3	Applications of ShakeMap	630
4.21.5.1.4	Global earthquake impact: PAGER	632
4.21.5.2	<b>Warnings before the Shaking</b>	632
4.21.5.2.1	S-waves versus P-waves	632
4.21.5.2.2	Single-station and network-based warnings	635
4.21.5.2.3	Warning around the world	635
4.21.5.2.4	ElarmS in California	636
4.21.5.2.5	Warning times	639
4.21.5.2.6	Future development	640
4.21.5.2.7	Benefits and costs	641
4.21.6	<b>Conclusion</b>	642
References		643

### 4.21.1 Introduction

Few natural events can have the catastrophic consequences of earthquakes, yet evidence abounds for repeating disasters in the same location. Archeological studies point to the recurring

destruction of Troy, Jericho, and Megiddo in the Mediterranean and the Middle East, and, in the New World, debris from the 1906 San Francisco earthquake was found beneath the destruction caused by the 1989 Loma Prieta earthquake in San Francisco’s Marina District.

Historical examples illustrate the sociopolitical impact of earthquakes. In 464 BCE, a powerful earthquake beneath the ancient Greek city Sparta led to the rebellion of Spartan slaves. According to Aristotle's *Politics* (1269a37-b5), these slaves were "like an enemy constantly sitting in wait for the disasters of the Spartans". The devastation that Sparta suffered from the earthquake offered them the perfect opportunity. The rebellion, which lasted for 10 years, limited Sparta's ability to check the growth of Athenian power in Greece and also led to the dissolution of the Spartan–Athenian alliance formed some 30 years earlier in the face of the Persian threat.

More recently, another natural disaster destroyed much of New Orleans and the Gulf coast of Louisiana. Few believed a natural hazard could be so devastating to a modern wealthy city, yet Hurricane Katrina flooded 80% of the city, much of which is below sea level, and destroyed over 300 000 housing units in August 2005. Despite a warning of the impending hurricane several days in advance, over 1800 people were killed. One year later, the population of the city is less than 50% of its previous level and it is clear that many will not return.

The challenge of natural hazard reduction generally, and earthquake hazard mitigation in particular, is the long return interval of these events. The infrequency of large seismic events provides only a limited data set for the study of earthquake impacts on modern cities, and the uncertainty as to when the next event will occur often places earthquake mitigation low on the priority list. The fields of seismology and earthquake engineering are also relatively juvenile, having only developed out of large destructive earthquakes at the end of the nineteenth and beginning of the twentieth centuries. Still, there has been considerable progress. Your chance of being killed in an earthquake is a factor of 3 less than it was in 1900.

Yet, earthquakes account for 60% of natural hazard fatalities today (Shedlock and Tanner, 1999). The number of people killed in earthquakes continues to rise in poorer nations, and the cost of earthquakes continues to rise for rich nations. The global population distribution is changing rapidly as underdeveloped nations continue to grow most rapidly in cities that are preferentially located in seismically hazardous regions. There has not yet been a large earthquake directly beneath one of these megacities, but when such an event occurs the number of fatalities could exceed 1 million (Bilham, 2004).

This chapter considers seismic hazard mitigation. First, we evaluate the hazard and risk around the

globe to identify where mitigation is necessary. Next, we consider the topic of earthquake prediction which is often called upon by the public as the solution to earthquake hazard. Instead, effective earthquake mitigation strategies fall into two groups, long- and short-term. We address long-term methods first, focusing on the use of earthquake-resistant buildings. In the past, their development has been largely reactive and driven by observed failures in most recent earthquakes. As testing of building performance in future earthquakes has become more viable, there is a potential for more rapid improvements to structural design. At the same time, however, the challenges of implementation will persist, leading to a widening implementation gap between the rich and poor nations. Short-term mitigation is the topic of the final section. Over recent years, modern seismic networks have facilitated the development of rapid earthquake information systems capable of providing hazard information in the minutes after an earthquake. These systems are now beginning to provide the same information in the seconds to tens of seconds prior to ground shaking. We consider possible future applications around the world.

## 4.21.2 Recognizing and Quantifying the Problem

### 4.21.2.1 Forecasting Earthquakes at Different Spatial and Temporal Scales

The first step in seismic hazard mitigation is identification and quantification of where the hazard exists. Today, plate tectonics provides the theoretical framework for identifying and characterizing seismic source regions: where earthquakes have occurred in the past, earthquakes will occur in the future. But before the development of plate tectonic theory in the late 1960s, the same concept was in use to forecast future earthquakes. In a letter to the *Salt Lake City Tribune* in 1883, G. K. Gilbert reported the findings of his field work along the Wasatch Front. He noted that the fault scarps were continuous along the base of the Wasatch with the exception of the segment adjacent to Salt Lake City where a scarp was missing. He concluded that there had been no recent earthquake on the section adjacent to the city, and this section was therefore closer to failure. In his study of deformation associated with the 1906 San Francisco earthquake, H. F. Reid built on Gilbert's model to develop elastic rebound theory which remains the

basis of our understanding of the earthquake cycle today (Reid, 1910). In the elastic rebound model, the relative motion between two adjacent tectonic plates is accommodated by elastic deformation in a wide swath across the plate boundary. Once the stress on the plate boundary fault exceeds the strength of the fault, rupture occurs and the accumulated deformation across the plate boundary collapses onto the fault plane.

This cyclicity to earthquake rupture is the basis of the seismic gap method of earthquake forecasting. If a fault segment fails in a quasi-periodic series of characteristic earthquakes, then the recurrence interval between events can be estimated either from the dates of past earthquakes or calculated by taking the characteristic slip during an earthquake and dividing by the long-term slip rate of the fault. Reported successes of seismic-gap theory include the deadly 1923 Kanto earthquake and the great Nankaido earthquakes of 1944 and 1946 (Aki, 1980; Nishenko, 1989). In 1965, Fedotov published a map showing where large-magnitude earthquakes should be expected, and his predictions were promptly satisfied by the 1968 Tokachi-Oki, 1969 Kuriles, and 1971 central Kamchatka earthquakes (Fedotov, 1965; Mogi, 1985). In the 1970s, the approach was applied around the globe. The estimates of relative plate motions provided by the new plate tectonic theory could be translated into slip rates across major faults. Once combined with data on the recent occurrence of large earthquakes, maps were generated identifying plate boundary segments with high, medium, and low seismic potential (Kelleher *et al.*, 1973; McCann *et al.*, 1979).

However, the utility of the seismic gap method for earthquake forecasting remains a topic of debate today (e.g., Nishenko, 1989; Kagan and Jackson, 1991; Nishenko, 1991; Jackson and Kagan, 1993; Nishenko and Sykes, 1993; Kagan and Jackson, 1995). Challenges to its practical application include the incomplete historic record of earthquakes making it difficult to estimate recurrence intervals, and difficulty in identifying the characteristic earthquake for a given fault segment. Earthquakes are also observed to cluster in space and time. Mogi (1985) proposed that plate boundary segments go through alternating periods of high and low activity, and the earthquake catalog suggests alternating periods of subduction versus strike-slip earthquake activity (Romanowicz, 1993). Laboratory experiments of stick-slip behavior show that rupture occurs at irregular intervals with variable stress drops. This implies that the state of

stress before and/or after each earthquake is also variable. In Reid's original development of elastic rebound theory, he forecast that the next earthquake should be expected when "the surface has been strained through an angle of 1/2000" (Reid, 1910). However, he also points out that this assumes a complete stress drop, that is, release of all accumulated strain, by the 1906 earthquake.

The Parkfield prediction experiment is one of the more famous applications of seismic gap theory. Three M 6 earthquakes located close to Parkfield in central California were instrumentally recorded in 1922, 1934, and 1966. Other data suggest an additional three events in 1857, 1881, and 1901 with a similar size and location. The similar recurrence interval of 22 years for the six events, the similar waveforms for the 1922, 1934, and 1966 events, and similar foreshock patterns prior to 1934 and 1966 make this one of the strongest cases for a characteristic earthquake (Bakun and McEvilly, 1979). Based on this evidence, Bakun and Lindh (1985) predicted that the next earthquake was due in 1988 with a 95% confidence that it would occur before 1993. An M 6.0 earthquake did occur on the Parkfield segment of the San Andreas, but not until September 28, 2004. While it had the same magnitude as previous events, the characteristics of its rupture were different (e.g., Langbein *et al.*, 2005).

These examples show that while the concept of recurring seismicity is useful for forecasting future seismic hazard, the application of a recurrence interval to predict the timing of the next earthquake is fraught with uncertainties. When viewed as a stationary series, past earthquake history can be used to forecast the probability of an earthquake over long time periods (hundreds of years), and this forms the basis of the probabilistic seismic hazard analysis discussed in the next section. However, as the spatial and temporal scales for the forecast become smaller, the uncertainties in those forecasts become greater. The challenge is to provide forecasts that are considered relevant by society, a society which at best plans for time periods of years to decades.

#### 4.21.2.2 Global Seismic Hazard

The United Nations designated the 1990s the International Decade of Natural Disaster Reduction. The Global Seismic Hazard Assessment Program (GSHAP) was part of this effort and had the goal of improving global standards in seismic hazard assessment (Giardini, 1999). From 1992 to 1998, an

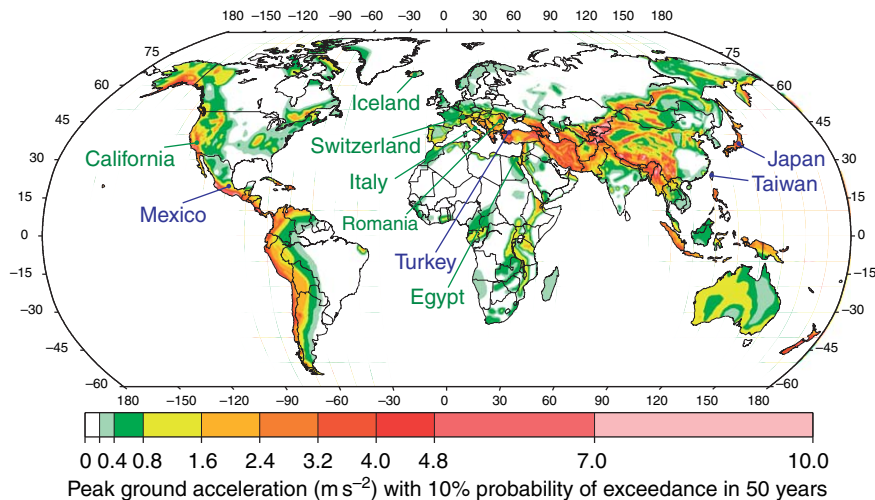


**Figure 1** The global seismic hazard map developed by the Global Seismic Hazard Assessment Program (Giardini, 1999). The map depicts PGA with a 10% probability of exceedance in 50 years, corresponding to a return interval of 475 years. The cooler colors represent lower hazard while the warmer colors are high hazard: white and green correspond to low hazard ( $0\text{--}0.08\text{ m s}^{-2}$ ); yellow and light orange correspond to moderate hazard ( $0.08\text{--}0.24\text{ m s}^{-2}$ ); darker orange corresponds to high hazard ( $0.24\text{--}0.40\text{ m s}^{-2}$ ); and red and pink correspond to very high hazard ( $>0.40\text{ m s}^{-2}$ ).

international collaboration of scientists conducted coordinated probabilistic seismic hazard analyses on a regional basis and combined them into the uniform global seismic hazard map shown in **Figure 1** (Giardini *et al.*, 1999). The maps present the levels of peak ground acceleration (PGA) with a 10% probability of exceedance (90% probability of nonexceedance) within 50 years, corresponding to a return period of 475 years. For more information on GSHAP, visit <http://www.seismo.ethz.ch/GSHAP/>.

Probabilistic seismic hazard analysis (PSHA) was first introduced by Cornell (1968). PSHA provides the relationship between some ground motion parameter, such as PGA, and its average return interval. There are three elements to the methodology. First, the seismic sources in a region must be characterized. It is necessary to determine where earthquakes occur, how often they occur, and how large they can be. Seismicity catalogs, both instrumental and preinstrumental, form the basis of this assessment. But these catalogs are inevitably incomplete with respect to geologic timescales. Additional geodetic and geologic data are therefore included when available. Second, the expected distribution of ground shaking for all possible earthquakes is estimated. This is usually achieved using attenuation relations which describe the level of ground shaking as a function of magnitude, distance, fault type, and local site conditions. The attenuation relations are determined by regression of peak ground shaking observations for past

earthquakes in the region. The quality of the attenuation relations is therefore data-limited, as we do not have observations of all possible earthquakes, particularly the larger infrequent events. For this reason, theoretical modeling of waveform propagation is now being used to improve our understanding of likely ground motions for the largest earthquakes. Finally, the probability of ground shaking at various levels is calculated by determining the annual frequency of exceedance.

To illustrate PSHA, consider the historic parameter method (Veneziano *et al.*, 1984; McGuire, 1993). A uniform earthquake catalog is developed for the region, and attenuation functions are identified. The expected ground motion for each earthquake is then determined at every site across the region. Return periods for exceedance of ground shaking at various levels can then be tabulated and plotted to generate a hazard curve. The curve provides ground shaking level versus recurrence interval, or, equivalently, probability of exceedance within some time window. The choice of ground shaking parameter varies. PGA is a short period ground motion parameter that is proportional to force and is the most commonly mapped as the seismic provisions of current building codes specify the horizontal force a building should withstand during an earthquake. It is also the most appropriate measure for the most common building type, one- and two-story buildings, as they have short natural

periods of typically 0.1–0.2 s. Other parameters that are used include peak ground velocity (PGV), which is more sensitive to longer periods and therefore appropriate for taller buildings (the natural period of buildings is typically 0.1 s per floor), and spectral response ordinates at various periods (0.3 s, 0.5 s, 1.0 s, 2.0 s, etc.), which are also related to the lateral forces that damage taller, longer period, buildings.

The GSHAP applied PSHA around the globe. While every effort was made to apply a uniform analysis, the differences in available data set inevitably result in some differences in the analyses for different regions (see Grunthal *et al.*, 1999; McCue, 1999; Shedlock and Tanner, 1999; Zhang *et al.*, 1999). Hazard curves were generated for all locations, and **Figure 1** shows the PGA with a 10% probability of exceedance within 50 years. The greatest hazard is adjacent to the major transform and subduction plate boundaries: around the Pacific rim, and through the broad east–west belt running from the Italian Alps, through Turkey, the Zagros Mountains of Iran, the Hindu Kush and Tian Shan, and then broadening to a wider belt including the region from the Himalaya to Siberia. High seismic hazard also wraps around the coastlines of the northeast Indian Ocean, where the 2004 Sumatra–Andaman earthquake and tsunami was responsible for an estimated quarter of a million deaths. The largest recorded earthquakes are all subduction zone events; the largest three events during the last century were the 1960 Chile ( $M_w$  9.5), 1964 Alaska ( $M_w$  9.2), and 2004 Sumatra–Andaman ( $M_w$  9.1) earthquakes. But the seismic hazard associated with major transform boundaries is just as large despite typically generating smaller earthquakes. This is due to the greater depth of large subduction zone earthquakes (tens of kilometers) and distance offshore, allowing attenuation of the seismic waves before they reach the land surface. By comparison, strike-slip faults rupture the shallow continental crust such as along the San Andreas Fault and the North Anatolian Fault.

#### 4.21.2.3 Changing Seismic Risk

##### 4.21.2.3.1 Earthquake fatalities since 1900

The new millennium has not started well in terms of earthquake impacts on society. As of October 2006, the twenty-first century has seen almost 400 000 deaths associated with earthquakes. This represents more than 20% of the estimated 1.8 million deaths during the entire twentieth century. There is no

evidence of any increase in seismic hazard; the number of earthquakes is not increasing. But, is there an increase in seismic risk?

Seismic hazard analysis provides information about the likelihood of earthquakes and associated ground shaking (**Figure 1**). But the hazard is distinct from the ‘seismic risk’, which represents the anticipated losses in a region either for a given scenario earthquake or for all anticipated earthquakes. Determination of the risk involves a convolution of the seismic hazard with population density and the properties of the built environment, including the number of buildings and the type of construction. Fragility curves are used to describe the likely damage to a building, or construction type, given different levels of ground shaking. Frequent, large earthquakes in remote areas represent high seismic hazard but low seismic risk, while moderate earthquakes directly beneath a large urban center can represent low hazard but high risk.

**Figure 2** shows the cumulative number of earthquake deaths since 1900. The data come from the Significant Earthquake Database (Dunbar *et al.*, 2006), edited to remove multiple entries and updated for the present paper. Statistical analysis of such data is notoriously difficult as it is dominated by infrequent high-fatality events. While there were 138 earthquakes with more than 1000 fatalities since 1900, the 10 events with the largest fatality rate caused over 60% of the deaths. The data show two trends, pre- and post- 1940 (**Figure 2**). Prior to 1940, fatalities occur at a rate of  $\sim 25$  000 per year; after 1940, the character changes and is dominated by two large

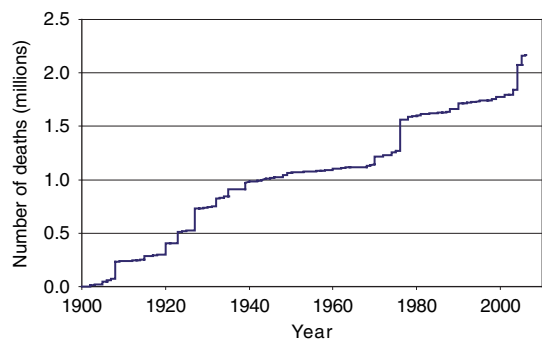


**Figure 2** Cumulative number of earthquake fatalities since 1900. Note the change in character pre- and post-1940. The annual rates are  $\sim 25$  000 per year pre-1940 and  $\sim 19$  000 per year post-1940. Post-1940 fatalities are dominated by the Tangshan (1976) and Sumatra (2004) events with lower rates ( $\sim 8000$  and  $\sim 9000$  per year) in between.

fatality events (Figures 2 and 3(a)) and lower fatality rates of  $\sim 8000$  per year from 1940 to 1976, and  $\sim 9000$  per year from 1976 to 2004. The 1976 Tangshan earthquake is the most recent in a series of earthquakes in China with very large numbers of fatalities. The 1920 Gansu and 1927 Tsinghai earthquakes both killed an estimated 200 000; another earthquake in Gansu Province killed 70 000 in 1932; and, finally, the Tangshan earthquake had an official death toll of 242 000 (as in Figure 2) but unofficial estimates as high as 655 000. The second major event in the post-1940 time series is the Sumatra earthquake and tsunami of 26 December 2004. The United Nations estimates 187 000 confirmed dead and an additional 43 000 missing. Most of these fatalities occurred in the Aceh Province of Indonesia, at the northern end of the island of Sumatra, and along the

Nicobar and Andaman Islands extending to the north along the subduction zone. Sri Lanka to the west and Thailand to the east were also heavily affected. The fatalities from this event are therefore more distributed than the other major events since 1900 on account of the broader reach of tsunami hazard.

The total fatality rate from 1940 to 2006 is  $\sim 19\,000$  per year, lower than the  $\sim 25\,000$  per year rate from 1900 to 1940. However, it would be a mistake to conclude that the earthquake-related fatality rate is declining as the post-1940 rate is dominated by just two events. In fact, the last five centuries of earthquake fatalities show an increasing rate. Using a best-fit power law and data from the last five centuries, Bilham (2004) estimates that the annual rate of earthquake fatalities continues to increase. While the number of deaths is increasing,

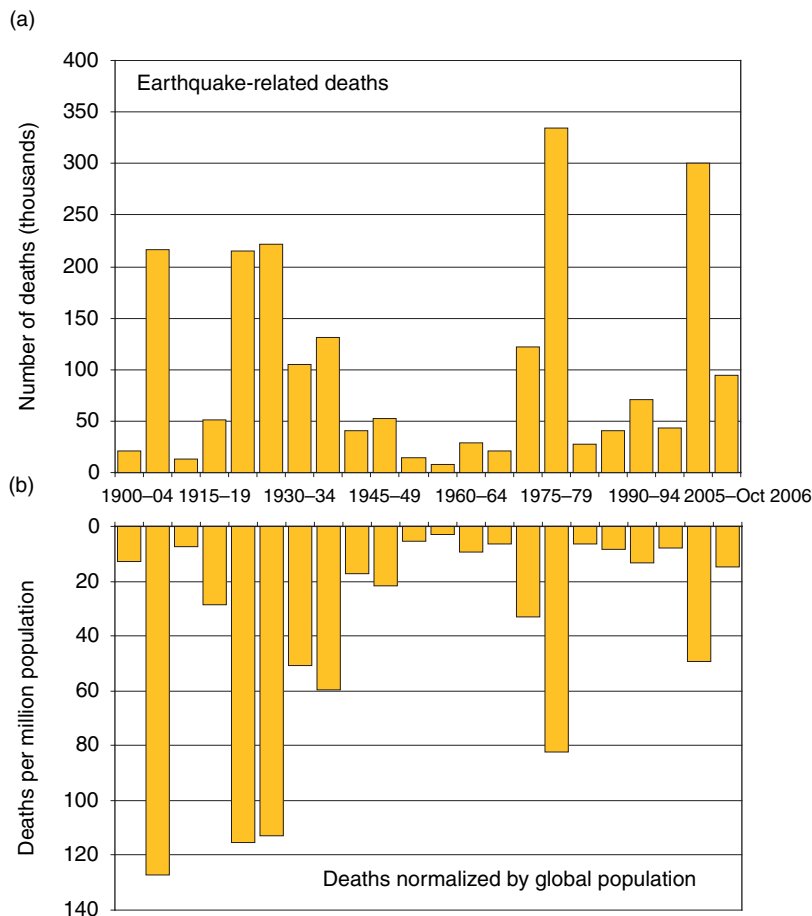


**Figure 3** Earthquake-related deaths since 1900 in 5 year bins. (a) Total number of deaths. (b) Deaths per million global population. While the intervals including the 1976 Tangshan and 2004 Sumatra events have the highest number of fatalities, once normalized by global population it is the first part of the twentieth century which has the highest rates with over 100 per million in three intervals.

it is not increasing as quickly as global population. Normalizing Bilham's best-fit annual fatality rate by global population, an individual's risk of dying in an earthquake has reduced by a factor of 2 since 1950 and a factor of 3 since 1900. This can also be seen when considering the fatalities during 5 year intervals as shown in **Figure 3**. The largest number of fatalities in these 5 year intervals was due to the 1976 Tangshan and 2004 Sumatra events. During these intervals, there were over 300 000 deaths, but once normalized by the global population the highest fatality rates were during the first part of the twentieth century, when there were more than 100 deaths per million population during three 5 year intervals (**Figure 3(b)**).

So, are the advances in earthquake science and engineering paying off? Are we living in a more earthquake-resilient world? This conclusion would be premature for several reasons. First, the fatality rate is dominated by large impact events, and a few such events in the coming decades would reverse this trend. Second, the application of earthquake mitigation strategies is highly uneven around the globe, resulting in very different trends in regional earthquake fatality rates. Third, the distribution of global population is changing rapidly, on shorter timescales than the earthquake cycle. While the more-developed nations show zero growth, rapid growth continues in the less-developed nations, particularly in the cities. Finally, it would be irresponsible to declare success in global earthquake mitigation when the annual number of fatalities continues to increase.

#### 4.21.2.3.2 Concentrations of risk

The high fatality rate earthquakes recur in a relatively small number of countries. Since 1900, the 12 earthquakes causing more than 50 000 fatalities have occurred in China, Pakistan, Iran, Indonesia, Japan, Italy, and Peru. Almost half of all earthquakes causing more than 1000 deaths have occurred in these seven countries. But the application of earthquake mitigation strategies is variable. In Japan, which has seen over 100 000 fatalities in the last century, most from the 1923 Tokyo earthquake and fire, stringent building codes are enforced, regular earthquake evacuation drills are carried out, and, most recently, an earthquake early-warning system was implemented. While in Iran, which experienced ~190 000 fatalities since 1900, the number of earthquake fatalities has tracked the population growth – one in 30 000 Iranians die in earthquakes – and the existence

of earthquake building codes has had little or no effect (Berberian, 1990; Bilham, 2004).

The introduction of the medicinal control of contagious diseases at the beginning of the twentieth century finally allowed rapid growth of urban centers. Since 1950, 60% of global population growth has occurred in urban centers, almost 50% in the lesser-developed nations (United Nations, 2004). Today, the global rural population is almost flat and the number of urban dwellers will exceed rural dwellers in 2007 for the first time. This is causing a rapid redistribution of the global population. Most of the population growth is now occurring in the less-developed nations. Within each nation, the population is migrating to the urban centers, particularly in the less-developed nations. In a series of papers, Bilham (1988, 1996, 1998, 2004) has pointed to this trend and cautioned that much higher numbers of fatalities from single events might be expected when an earthquake strikes beneath one of the growing number of large urban agglomerations.

This migration of population to the cities results in concentrations of risk. As the number of cities grows, the likelihood that an earthquake will strike a city also grows. In addition to this trend, the global distribution of the world's largest urban centers is changing. The largest cities today are in locations with a greater seismic risk than the largest cities in 1950. **Figure 4** shows the seismic hazard for the world's 30 largest urban centers in 1950, 1975, 2000, and 2015. It shows that while only 10 were in regions of moderate to high hazard in 1950, this number had increased to 16 by 2000, and the trend is projected to continue. Most of the change occurred by adding new cities to the top 30 in regions of high hazard, while cities with a low hazard dropped off the list; the number of moderate hazard cities remains fairly constant. The geographic distribution of the 30 largest urban centers is shown in **Figure 5**. The reason for the changing hazard is clear. While the growth of cities in northern Europe and the northeastern United States has been relatively slow, rapid growth of cities in western South America and across Asia has propelled these cities with higher seismic hazard into the top 30 list.

It is tempting to associate the changing trend of global earthquake fatalities (**Figure 2**) with the growth of cities. Pre-1940 earthquake fatalities are more constant, while most fatalities post 1940 occurred in two events. One of the two events, 1976 Tangshan, was beneath a large city, but the fatalities in the 2004 Sumatra event were more distributed due

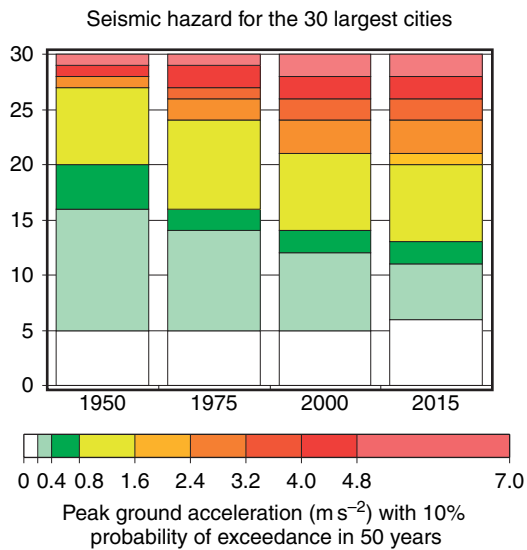


**Figure 4** Seismic hazard for the 30 largest cities in 1950, 1975, 2000, and 2015 (projected). City population data from the United Nations. The seismic hazard at each city location is provided by the GSHAP map and represented as PGA with a 10% probability of exceedance in 50 years. The chart shows that cities in seismically safe regions are removed from the top 30 list as cities in hazardous regions grow more rapidly.

to the tsunami. The shortness of the time history makes it impossible to be certain of the cause, and there has not yet been a large earthquake beneath a megacity.

#### 4.21.2.4 Local Hazard and Risk: The San Francisco Bay Area

##### 4.21.2.4.1 The San Francisco Bay Area

All seismic hazard mitigation occurs on a local scale. For this reason, it is useful to consider a case example such as the San Francisco Bay Area (SFBA). The SFBA sits within the Pacific–North America plate boundary, which takes the form of multiple fault strands through the region (**Figure 6**). The interseismic displacement between the Pacific Plate and the western edge of the Central Valley is  $38 \text{ mm yr}^{-1}$ , representing approximately 80% of the motion between the Pacific and North American Plates (d'Alessio *et al.*, 2005). This narrow strip of land that forms the Coast Ranges of California is only  $\sim 100 \text{ km}$  wide but has a population approaching 7 million concentrated around the bay. The SFBA has

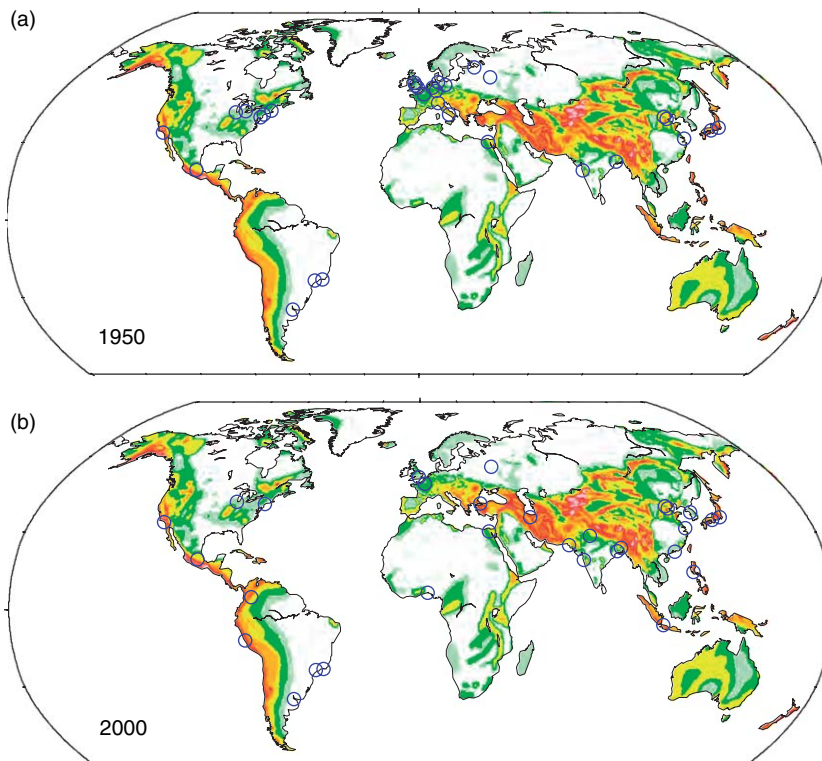


**Figure 5** The locations of the 30 largest cities in (a) 1950 and (b) 2000 (blue circles) superimposed on the GSHAP hazard map. The increased seismic hazard for the largest cities is due to relatively slow growth of cities in the eastern US and northwest Europe while cities across Asia grow more rapidly.

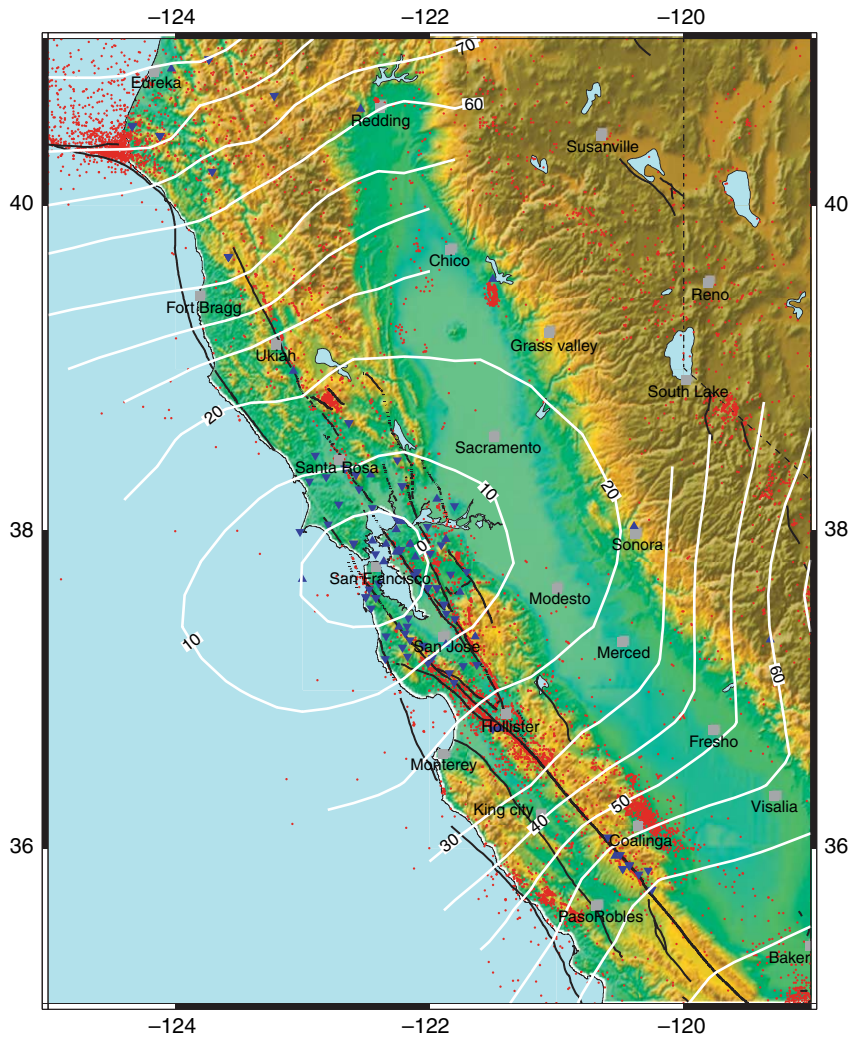


**Figure 6** Map of northern California showing topography (color pallet), faults (black lines), earthquakes (red dots), seismic stations available for early warning (blue triangles and diamonds) and the warning time San Francisco could expect for earthquakes at all locations across the region (white contours, time in seconds). The warning time is estimated using ElarmsS and the current seismic network and telemetry. There would be greatest warning for earthquake furthest away from the city. The existing seismic stations shown are operated by UC Berkeley and the US Geological Survey.

the highest density of active faults and the highest seismic moment rate per square kilometer of any urban area in the United States (WG02, 2003).

The historic earthquake record is short, believed to be complete for  $M \geq 5.5$  since 1850, at which time the population exploded after gold was found in the Sierra foothills (Bakun, 1999). Some information is available back to 1776 when the first Spanish mission, Mission Delores, was founded. The record contains six  $M \geq 6.5$  earthquakes in the SFBA in 1836, 1838, 1865, 1868, 1906, and 1989, four in the 70 years prior to 1906 and only one in the 100 years since. This change in the seismic energy release rate is believed to be due to the ‘stress shadow’ resulting

from the 1906 earthquake (Harris and Simpson, 1998). The 1906 event ruptured the northernmost 450 km of the San Andreas Fault from San Juan Bautista to Cape Mendocino extending through the SFBA and destroying much of San Francisco and Santa Rosa to the north. As most faults in the SFBA share a subparallel, strike-slip geometry to the San Andreas Fault, they were relaxed by the 1906 rupture.

Mapping active faults in California is the responsibility of the California Geological Survey (CGS). Under the 1972 Alquist-Priolo Earthquake Fault Zoning Act, all faults that have ruptured within the last 11 000 years are considered active, and building

close to these known faults is tightly regulated to ensure that buildings are at least 50 feet from the fault trace. The CGS is now also in the process of mapping other seismic hazards including liquefaction and landslide hazards during earthquakes.

The Southern California Earthquake Center (SCEC) is a collaboration of earthquake scientists working with the goal of understanding the earthquake process and mitigating the associated hazards. While SCEC is focused on the earthquake problem in southern California, the methodologies developed by SCEC scientists to quantify earthquake probabilities and the shaking hazards associated with them are applicable everywhere, including in our chosen region of focus, the SFBA.

#### 4.21.2.4.2 Earthquake probabilities

To evaluate the probability of future earthquakes and ground shaking in the region, the US Geological Survey established a Working Group on Earthquake Probabilities. In several incarnations starting in 1988, the group has collected data and applied the most up-to-date methodologies available to estimate long-term earthquake probabilities drawing on input from a broad cross section of the Earth science community. The most recent study (hereafter WG02) was completed in 2002 (WG02, 2003). In it, the probabilities of one or more earthquakes in the SFBA, on one of the seven identified fault systems, between 2002 and 2032 were estimated. The likely intensities of ground shaking were also combined to produce a probabilistic seismic hazard map for the region, similar to the GSHAP map discussed above. The WG02 results are shown in Figure 7.

The earthquake model used to estimate these probabilities has three elements. The first is a time-independent forecast of the average magnitudes and rates of occurrence of earthquakes on the major identified fault segments. It is derived from the past earthquake catalog. The second element includes four time-dependent models of the earthquake process to include the effects of the earthquake cycle and interactions between the fault systems. The concept of the earthquake cycle holds that after a major earthquake and associated aftershocks, another major rupture is not possible until the elastic strain has reaccumulated (Reid's elastic rebound theory). As time goes by, the probability of an earthquake therefore increases. A major earthquake also reduces the stress on any adjacent faults with a similar orientation, generating a stress shadow. This has been observed both in

numerical models and in the reduced seismicity on faults adjacent to the San Andreas after the 1906 rupture. In the SFBA, both the 1906 event and the more recent 1989 earthquake cast stress shadows. The third element of the earthquake model characterizes the rates of background seismicity, that is, earthquakes that do not occur on the seven major fault systems. The 1989 Loma Prieta event was one such earthquake. These various earthquake models provide different estimates of earthquake probabilities. WG02 uses expert opinion to determine the relative weight for each probability estimate derived from each model.

Figure 7 shows the WG02 results. It is estimated that there is a 62% probability of one or more  $M \geq 6.7$  earthquakes in the SFBA from 2002 to 2032. As shown in Figure 7(a), the probability of one or more  $M \geq 6.7$  events is greatest on the Hayward–Rodgers Creek and San Andreas Faults, which have probabilities of 27% and 21%, respectively. The estimated uncertainties in these numbers are substantial. For the SFBA the 95% confidence bounds are 37% to 87%. For the Hayward–Rodgers Creek and San Andreas Faults, the bounds are 10–58% and 2–45%, respectively. A critical source of this uncertainty is the extent to which the SFBA has emerged from the stress shadow of the 1906 earthquake. Simple elastic interaction models suggest that the region should have emerged from the stress shadow, while the low seismicity rates for the last century would suggest that the SFBA remains within the shadow. Rheological models of the crust and uppermost mantle, and perhaps the 1989 Loma Prieta earthquake, suggest that the region may just be emerging now. If the region is emerging, then it can expect an increase in the number of major events over the next few decades.

#### 4.21.2.4.3 Future losses

Just as the world has not experienced a major earthquake beneath a megacity, the US has not experienced a major earthquake directly beneath one of its cities. The two most damaging earthquakes were the 1989 Loma Prieta earthquake (which was beneath the rugged mountains 100 km south of San Francisco and Oakland) and the 1994 Northridge earthquake (which, although centered beneath the populated San Fernando Valley, caused strongest ground shaking in the sparsely populated Santa Suzanna Mountains to the north). Each event caused ~60 deaths and the estimated damages were \$10 and

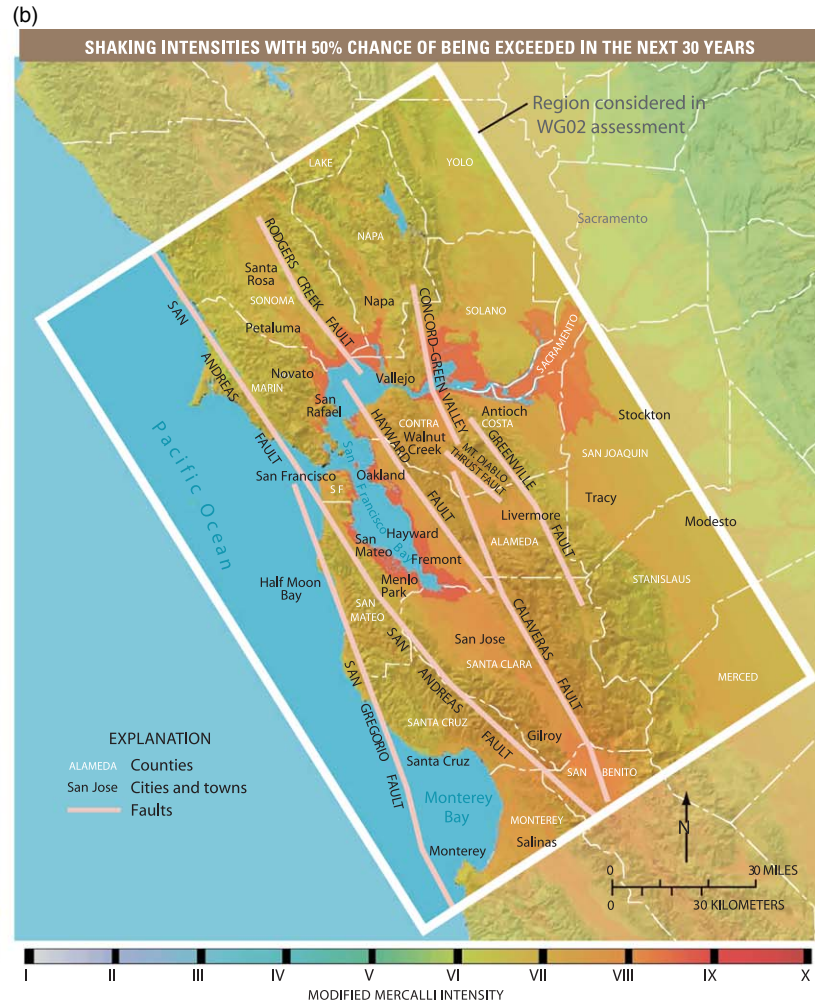
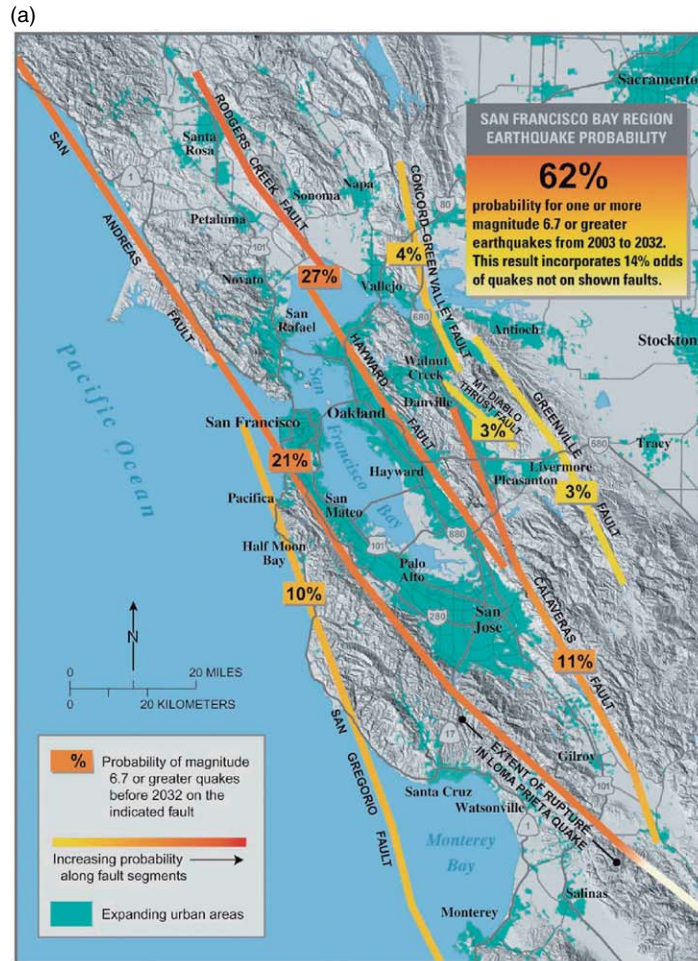


**Figure 7** (a) Map of the San Francisco Bay Area (SFBA) showing the urban areas and the probabilities of  $M \geq 6.7$  earthquakes by 2032. The probability of such an event in the SFBA is 62%, the probabilities of an  $M \geq 6.7$  earthquake on each fault are also indicated. (b) Shaking intensities with a 50% probability of exceedance by 2032. The soft sediments and landfill around the bay and delta are where the shaking hazard is the greatest. Both figures are taken from USGS Fact Sheet 039-03 (2003).

\$46 billion for Loma Prieta and Northridge, respectively (in 2000-dollars). While the impacts were significant, the events were relatively moderate in damage.

The ground shaking estimates, such as those that are part of WG02, provide the basis for loss estimation. Loss estimation methodologies use data on the locations and types of buildings, ground shaking maps for scenario or past earthquakes, and fragility curves relating the extent of damage to the ground shaking for each building type, to estimate the total damage from the event. The worst-case scenario considered for northern California is a repeat of the 1906 earthquake. The losses have been estimated at \$170–225 billion for all related losses including secondary fires and toxic releases (RMS, 1995), a factor of 2 greater than the \$90–120 billion loss estimate for property alone (Kircher *et al.*, 2006). It is estimated that the number of deaths could range from 800 to 3400 depending on the time of day, and 160 000–250 000 households will be displaced (Kircher *et al.*, 2006). An earthquake rupturing the length of the Hayward–Rodgers Creek Fault is estimated to cause \$40 billion in damage to buildings alone (Rowshandel, 2006).

These estimates of seismic hazard and risk provide a quantitative basis for earthquake hazard mitigation in the region. The choice of a relatively short, 30-year time window by WG02 has the advantage that it is a similar timescale to that of property ownership. But, as pointed out above and by WG02, the reliability of PSHA analysis decreases as the temporal and spatial scales decrease. Our observations of large ( $M > 6.5$ ) earthquakes in California are limited. Many of the recent damaging earthquakes occurred on faults that had not been recognized, including the two most damaging earthquakes, the 1989 Loma Prieta and 1994 Northridge events. While ‘background seismicity’ is included in the seismic hazard estimates, these events are a reminder of the limitations to our current understanding of the earthquake hazard. These hazard and risk estimates are therefore most appropriately used to motivate broad efforts to mitigate seismic hazard across the entire SFBA rather than efforts along a specific fault segment. The limitations in our observational data set also caution against becoming too ‘tuned’ in mitigation strategy. The use of multiple mitigation strategies will prevent over-reliance on a single, and possibly limited, model of future earthquake effects.

### 4.21.3 The ‘Holy Grail’ of Seismology: Earthquake Prediction

“When is the big one?” is the first question asked by every member of the public or press when they visit the Berkeley Seismological Laboratory. Answering this question, predicting an earthquake, is often referred to as the Holy Grail of seismology. In this context, a prediction means anticipating the time, place, and magnitude of a large earthquake within a narrow window and with a high enough probability that preparations for its effects can be undertaken (Allen, 1976). For the general public, answering this question is the primary responsibility of the seismological community.

The public considers earthquake prediction important because it would allow evacuation of cities and prevention of injury and loss of life in damaged and collapsed buildings. However, the seismology and engineering communities have already developed a strategy to prevent building collapse by identifying the likely levels of ground shaking and designing earthquake-resistant buildings that are unlikely to collapse. Once building codes for earthquake-resistant buildings are fully implemented, earthquake prediction would not be as important. But even before full implementation of building codes, earthquake prediction would only be partially successful as it would be capable of mitigating immediate and not long-term impacts of earthquakes. A prediction would allow for evacuations, but the ensuing earthquake would leave the urban area uninhabitable and only a fraction of the prior occupants would likely return.

It is possible to make high-probability short-term predictions for hurricanes as was done in the case of Hurricane Katrina in August 2005. Still, an estimated 1800 people were killed when New Orleans and other areas of Louisiana and Mississippi were inundated by flood waters. In New Orleans, 80% of the city was flooded, destroying much of the housing and infrastructure, and it is not yet clear what proportion will be replaced. One year later, the population of New Orleans was less than half its pre-Katrina level and roughly equivalent to what it was in 1880. If the built environment was designed to withstand a hurricane of Katrina’s strength, these lives would not have been lost and New Orleans would still be thriving.

For the scientific community, earthquake prediction has a much broader meaning, encompassing

the physics of the earthquake process at all time-scales. The long-term probabilistic forecasts described in the previous section are predictions, but they have low probabilities of occurrence over large time windows. There is currently no approach that has consistently predicted large-magnitude earthquakes and most seismologists do not expect such short-term predictions in the foreseeable future. While many advances have been made in understanding crustal deformation, stress accumulation, rupture dynamics, friction and constitutive relations, fault interactions, and linear dynamics, a lack of understanding of the underlying physics and difficulty in making detailed field observations mapping the spatial and temporal variations in structure, strain, and fault properties makes accurate short-term predictions difficult.

In addition to these observational constraints, earthquakes are part of a complex process in which distinct structures such as faults interact with the diffuse heterogeneity of the Earth's crust and mantle at all scales. Even simple mechanical models of the earthquake process show chaotic behavior (Burridge and Knopoff, 1967; Otsuka, 1972; Turcotte, 1992), suggesting it will be difficult to predict earthquakes in a deterministic way. Instead, it may only be possible to make predictions in a statistical sense with considerable uncertainty (Turcotte, 1992). Kanamori (2003) details the important sources of uncertainty: (1) the stress accumulation due to relatively constant plate motion can be modified locally by proximal earthquakes; (2) the strength of the seismogenic zone may change with time, say due to the migration of fluids; (3) predicting the size of an earthquake may be difficult depending on whether a small earthquake triggers a large one; (4) external forces may trigger events as observed in geothermal areas after large earthquakes.

Despite these challenges, the search for the silver bullet – an earthquake precursor – continues. As pointed out by Kanamori (2003), there are two types of precursors. For the purpose of short-term earthquake prediction, identification of a single precursor before *all* large magnitude events is desirable. To date, no such precursor has been identified as far as we know. However, unusual precursory signals have been observed before one, or perhaps a few earthquakes. These precursors may be observed before future earthquakes and are therefore worthy of research effort. The list of observed precursors includes increased seismicity and strain, changes in seismic velocities, electrical resistivity and potential, radio

frequency emission, and changes in ground water levels and chemistry (see Rikitake, 1986).

The one successful prediction of a major earthquake was prior to the 1975 M<sub>S</sub> 7.3 Haicheng (China) event. More than 1 million people lived near the epicenter, and a recent evaluation of declassified documents concludes that an evacuation ordered by a local county government saved thousands of lives (Wang *et al.*, 2006). There were two official middle-term predictions (1–2 years). On the day of the earthquake, various actions taken by provincial scientists and government officials constituted an imminent prediction, although there was no official short-term (a few months) prediction. A foreshock sequence consisting of several hundred events triggered the imminent prediction; other precursors including geodetic deformation, changes in groundwater level, chemistry, and color, and peculiar animal behavior are also reported to have played a role (Wang *et al.*, 2006). What is not known is how many false predictions were made prior to the evacuation, nor is it known how many earthquake evacuation orders have been made across China. The initial euphoria over the successful evacuation was soon dampened by the Tangshan earthquake the following year for which there was no prediction.

Extensive literature exists detailing the specifics of the various proposed earthquake prediction methodologies and other reported cases of earthquake prediction (Rikitake, 1976; Vogel, 1979; Wyss, 1979; Isikara and Vogel, 1982; Rikitake, 1982; Unesco, 1984; Mogi, 1985; Rikitake, 1986; Gupta and Patwardham, 1988; Olson *et al.*, 1989; Wyss, 1991; Lomnitz, 1994; Gokhberg *et al.*, 1995; Sobolev, 1995; Geller, 1996; Knopoff, 1996; Geller, 1997; Geller *et al.*, 1997; Sykes *et al.*, 1999; Rikitake and Hamada, 2001; Kanamori, 2003; Ikeya, 2004). Expert panels are used in many countries to evaluate earthquake predictions and provide advice to governments and the public. In the US, the National Earthquake Prediction Evaluation Council (NEPEC) provides advice to the director of the US Geological Survey, and the California Earthquake Prediction Council (CEPEC) advises the Governor. No short-term earthquake predictions have been made by these councils to date.

#### 4.21.4 Long-Term Mitigation: Earthquake-Resistant Buildings

The implementation of building codes mandating the use of earthquake-resistant buildings has been highly

successful in mitigating the impact of earthquakes in some regions. The number of fatalities has been reduced, and the majority of direct economic losses in recent US earthquakes (e.g., 1989 Loma Prieta, 1994 Northridge, and 2001 Nisqually) were from damage to buildings and lifelines constructed before 1976 when the Uniform Building Code was updated following the 1971 San Fernando earthquake (National Research Council, 2003). In the past, the improvement of building design was undertaken in response to observations from previous earthquakes. While improvements are still largely in response to past earthquakes today, new seismological and engineering techniques allow the development of design criteria for future likely earthquakes. Building design is also going beyond the prevention of collapse with the goal of reducing the costs of future earthquakes in addition to the number of fatalities. One of the challenges is implementation of earthquake-resistant designs, both for new construction and for the existing building stock.

#### 4.21.4.1 Earthquake-Resistant Design

##### 4.21.4.1.1 Lateral forces

Following the 1891 Nobi, Japan, earthquake that killed 7000 people, John Milne laid the foundation for the building codes that were to follow (Milne and Burton, 1891). He detailed the poor performance of modern masonry construction which had recently been introduced to replace the more traditional wood construction in an effort to mitigate fires, and described the great variability in damage to buildings over short distances due to the effect of soft versus hard ground. He also emphasized the need to design buildings to withstand the horizontal forces associated with earthquakes rather than just vertical forces. Similar observations were made following the 1906 San Francisco earthquake by the Lawson Commission (1908).

After the 1908 Messina-Reggio earthquake in southern Italy, which killed 83 000, Panetti proposed that buildings be designed to withstand a horizontal force in proportion to their vertical load. He suggested that the first story should be able to withstand 1/12th the weight of the overlying stories and the second and third stories should be able to withstand 1/8th (Housner, 1984). In Japan, Toshikata Sano made a similar proposal. In 1915, he recommended that buildings should be able to withstand a lateral force,  $V$ , in proportion to their weight,  $W$ , such that  $V = CW$ , where  $C$  is the lateral force coefficient

expressed as a percentage of gravitational acceleration. But it was not until the 1923 Kanto earthquake which killed 100 000 that Sano's criteria became part of the Japanese Urban Building Law Enforcement Regulations released in 1924 (Whittaker *et al.*, 1998). In the Japanese regulations,  $C$ , was set at 10%  $g$ . Following the 1925 Santa Barbara earthquake in the US, several communities adopted Sano's criteria with  $C = 20\%g$ . Sano's recommendation was also adopted in the first release of the US Uniform Building Code in 1927, where the value of  $C$  was dependent on the soil conditions (National Research Council, 2002).

##### 4.21.4.1.2 Strong-motion observations

While building codes were mandating earthquake-resistant designs as early as the 1920s, there were still no instrumental observations of the actual ground motions responsible for building damage. Milne and colleagues designed and built the first effective seismographs in Japan in the late 1880s. The first instruments in the US were installed at the Lick Observatory of UC Berkeley in 1887 (Lawson, 1908). By the 1920s, seismological observatories had been established around the world, but they were designed to measure the weak (low-amplitude) motion resulting from distant earthquakes. It was not until the 1930s that broadband strong (high-amplitude) motion instruments were available, capable of recording both the low- and high-frequency shaking responsible for the damage to buildings. The 1933 Long Beach earthquake provided the first instrumental recording in which PGAs of 29% $g$  in the vertical and 20% $g$  in the horizontal were observed. A larger PGA value of 33% $g$  was observed at EI Centro a few years later on an instrument 10 km from the 1940 M 7.1 Imperial Valley earthquake rupture. This remained the largest measured ground motion for 25 years, establishing the EI Centro seismogram as the standard for earthquake engineering in both the US and Japan.

Over the following decades, the strong-motion database grew, but slowly. This changed in 1971 when the M 6.6 San Fernando earthquake struck the Los Angeles region and the number of strong-motion recordings more than doubled. In this earthquake, more than 400 000 people experienced PGA in excess of 20% $g$ , and it became clear that high-frequency PGA varied over short distances while the longer period (10 s) displacements did not (National Research Council, 1971; Hudson, 1972; Hanks, 1975). One instrument located on the abutment of the Pacoima Dam recorded a  $1 \text{ m s}^{-1}$  velocity pulse

shortly followed by a 120%g acceleration pulse (Boore and Zoback, 1974). The strong-motion database generated by this earthquake played an important role in the updates to the Universal Building Code, which followed in 1976. It is a testament to the importance of strong-motion networks, and the earthquake engineering research they provide for, that the majority of damage in recent US earthquakes (1989 Loma Prieta, 1994 Northridge, and 2001 Nisqually) occurred to structures built prior to the 1976 update to the Uniform Building Code (National Research Council, 2003).

Strong-motion networks continue to provide important waveform data sets for damaging earthquakes. One notable recent example was the 1999  $M_w$  7.6 Chi-Chi earthquake, which occurred beneath central Taiwan on 20 September 1999. The strong-motion seismic network that had recently been deployed by the Central Weather Bureau across the island provided waveforms at 441 sites, including over 60 recordings within 20 km of the fault ruptures (Lee *et al.*, 2001). In addition to Taiwan, dense strong-motion networks with hundreds of instruments are now operational in Japan and the western US. Many more smaller networks are operational in earthquake prone regions around the world. They all provide crucial data when a large earthquake occurs close by, yet the infrequency of such events makes continuous funding and operation a challenge.

#### 4.21.4.1.3 Strong-motion simulations

Advances in computational capabilities, numerical techniques, and our knowledge of the structure of fault zone regions now make it feasible to simulate earthquakes to provide estimates of likely ground motions in future events. The recent centennial of the 1906 San Francisco earthquake motivated one such study in northern California. In order to simulate ground shaking, a velocity model was first developed for northern California. The geology-based model provides three-dimensional (3-D) velocity and attenuation for the simulation using observed relationships between rock type, depth, and seismic parameters (Brocher, 2005). Seismic and geodetic data available from the 1906 earthquake were used to map the distribution of slip in space and time on the fault plane (Song *et al.*, 2006). Several numerical techniques were then used to simulate the earthquake rupture through the geologic model. The simulations could be calibrated by comparing the calculated peak intensities with observed intensities from the 1906 earthquake which were compiled into

a 1906 ShakeMap (Lawson, 1908; Boatwright and Bundoock, 2005). Snap-shots from one of the simulations are shown in Figure 8, (Aagaard, 2006). The peak intensities generated by the simulations reproduce the prominent features of the 1906 ShakeMap validating the simulations.

Other simulations of the 1989 Loma Prieta earthquake, for which instrumental recording of ground shaking is available, also demonstrate that the simulations replicate the amplitude and duration of the observed shaking at frequencies less than 0.5 Hz (Aagaard, 2006; Dolenc *et al.*, 2006). Given likely slip distributions of future earthquakes, these simulations can now provide estimates of the ground shaking in the form of complete seismic waveforms. The results of one study on the southern San Andreas Fault are shown in Figure 9 (Olsen *et al.*, 2006). The source rupture is along the San Bernardino Mountains and Coachella Valley segments, which are considered more likely to rupture in the coming decades as they have not ruptured since 1812 and 1960. The slip distribution of the 2002  $M_w$  7.9 Denali, Alaska, earthquake was used for the rupture after scaling it for an  $M$  7.7 rupture. The velocity structure was provided by the SCEC Community Velocity Model (Kohler *et al.*, 2003), and ground shaking is calculated for frequencies of 0–0.5 Hz just as in the northern California simulations. When the rupture propagates from the southeast to the northwest, the directivity effect produces large amplitude ground motions in the Los Angeles metropolitan region. When the fault rupture is to the east of Los Angeles, the chain of sedimentary basins (the San Bernardino, Chino, San Gabriel, and Los Angeles basins) running westward from the northern termination of the rupture funnels seismic energy toward the downtown. The seismograms superimposed on Figure 9 show velocities of more than  $3 \text{ ms}^{-1}$ . When the rupture propagates to the southeast, the ground shaking in LA is an order of magnitude smaller (Olsen *et al.*, 2006).

These simulations are providing new insights into seismic wave propagation and help identify the geologic structures that control strong ground shaking. The uncertainties in the predicted ground shaking result from limitations in the velocity models, the numerical techniques, and the unknown future slip distributions. However, these simulations allow us to explore the range of possible ground motions that we might expect for earthquake ruptures that are evident in the geologic record but not the historic or instrumental records.

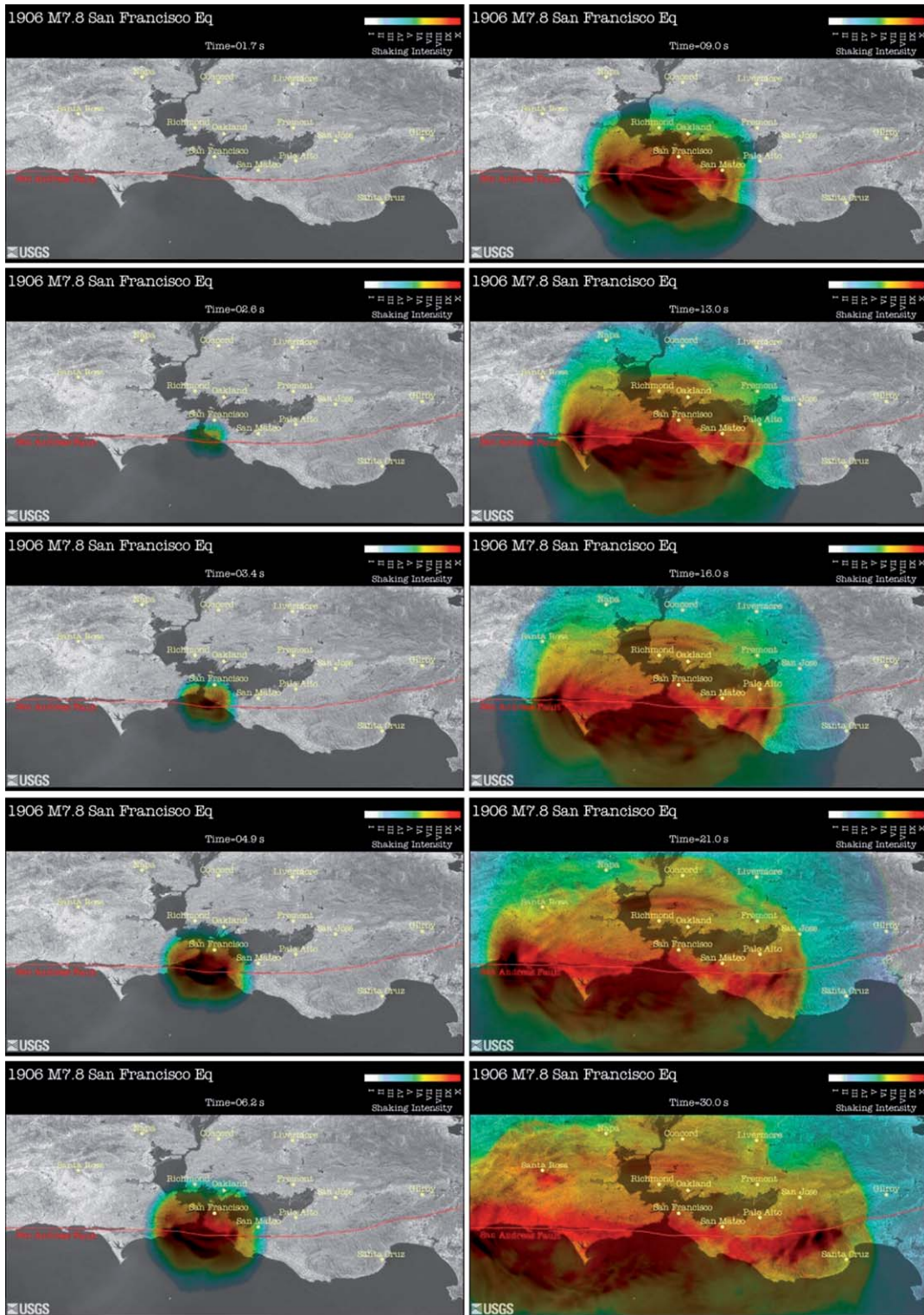


**Figure 8** Simulation of the 1906 rupture along the San Andreas Fault. Each map shows the San Francisco Bay Area, north is to the left, and the San Andreas Fault in red. The sequence of snapshots show the peak ground shaking intensity (MMI) 1.7, 2.6, 3.4, 4.9, 6.2, 9.0, 13.0, 16.0, 21.0 and 30.0 s after the rupture initiates. Figures provided by Brad Aagaard (2006). See <http://earthquake.usgs.gov/regional/nca/1906/simulations/>.

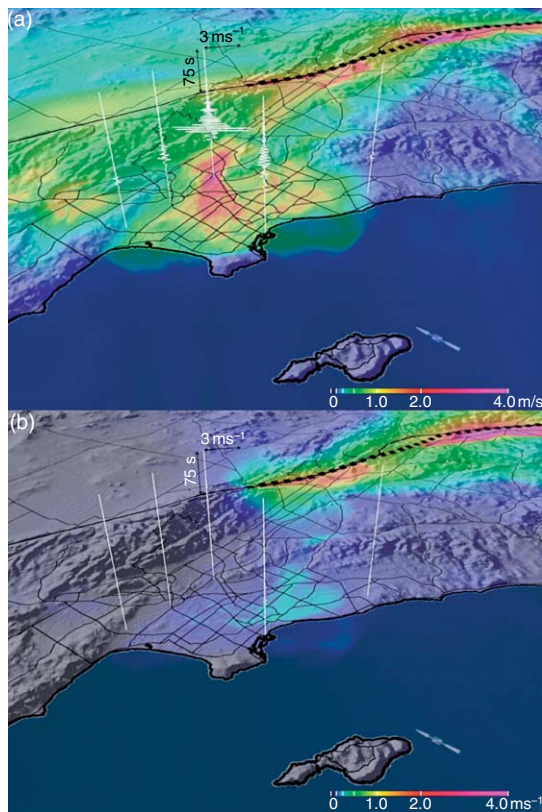


**Figure 9** Simulation of an M 7.7 rupture on the southernmost segments of the San Andreas Fault. The section of the fault to rupture is shown by the string of black squares. The color pallet shows the peak ground velocity. (a) Rupture from the south to the north showing the funneling of energy toward the Los Angeles basin west of the rupture. (b) When rupturing from north to south, the amplitudes in the Los Angeles basin are an order of magnitude smaller. From Olsen, *et al.* (2006) Strong shaking in Los Angeles expected from southern San Andreas earthquake. *Geophysical Research Letters* 33: L07305.

#### 4.21.4.1.4 New seismic resistant designs

As strong-motion waveforms became available to the engineering community, the complexity of surface ground motions and their interaction with buildings became apparent. Rather than containing a dominant period, the seismic waveforms were found to be more like white noise over a limited frequency range. Housner *et al.* (1953) proposed to reduce waveforms to a response spectrum, which is the maximum response of single degree-of-freedom oscillators with different natural periods and (typically) 5% internal damping to a recorded waveform. When the response is multiplied by the effective mass of a building, it constrains the lateral force the building would experience and should therefore be able to sustain.

The response spectra are still widely used today, but numerical techniques now allow for much more complex nonlinear modeling of buildings during ground shaking. Such modeling allows testing of new seismic resistant designs using past earthquake recordings as well as future earthquake scenarios. The 1994  $M_W$  6.7 Northridge earthquake in southern California exposed a vulnerability in steel moment frame buildings. Moment frames resist the lateral forces in an earthquake through bending in the rigidly connected beams and columns. Due to construction practices and the use of nonductile welds, a substantial number of connections fractured in the earthquake. The Universal Building Code was updated accordingly in 1997 (UBC97). But the question remains as to how these building will behave in a future larger magnitude earthquake. Krishnan *et al.* (2006) explored this question using a numerical simulation of two  $M_W$  7.9 earthquakes on the section of the San Andreas that last ruptured in 1857. They first calculated synthetic waveforms at various locations across southern California, and then simulated the effect of the ground shaking at each location on two 18-story steel moment frame buildings, one based on pre-UBC97 code, and one that was post-UBC97. Krishnan *et al.* concluded that if the rupture propagated north-to-south (toward Los Angeles), then the pre-UBC97 building would likely collapse in the San Fernando Valley, Santa Monica, west Los Angeles, Baldwin Park, Compton, and Seal Beach. The post-UBC97 building would likely survive in most locations except the San Fernando Valley. This type of modeling is currently confined to the academic community; however, there is the potential to bring the lessons learned to bear on future construction practices.

Building codes for most buildings are currently focused on 'life safety', the prevention of fatalities in an earthquake. Fatalities mostly occur due to building collapse. The goal of building codes is therefore to prevent collapse in order to get everyone out alive. With a few exceptions, codes are not intended to keep buildings in service after an earthquake and a building that performed 'well' may still need to be demolished. Earthquake engineering is now looking beyond life safety to further reduce the damage to a building at specific levels of ground shaking. Performance-based seismic design (PBSD) is one approach which focuses on what to achieve rather than what to do. The implementation of PBSD concepts will therefore lead to buildings that combine the current prescriptive building codes to prevent

collapse with owner-selected design components to reduce the damage to economically acceptable levels. As a result, we can expect not only reduced fatalities in future earthquakes but also reduced economic losses which would be a reversal of the current trend of increasing economic losses (National Research Council, 2003). This poses challenges for both the seismological and engineering communities. While it is the low-frequency energy that is responsible for damage to buildings, damage to the building content is more sensitive to higher frequencies, greater than the frequency content of current ground motion simulations. For the engineering community, PBDS requires much more detailed knowledge of the performance of building components than the current prescriptive methods.

Building code requirements for critical facilities such as nuclear power plants, dams, hospitals, bridges, and pipelines are usually greater than the life safety standard currently used for homes and offices. The design criteria are continued operation for safety reasons, for example, dams and nuclear power plants, or to provide recovery services in the aftermath of an earthquake, for example, hospitals. The engineering of these facilities is usually site specific. One example of successful engineering of a critical facility is the Trans-Alaska Pipeline, a 48-inch diameter pipeline carrying over 2 million barrels of North Slope oil to the Marine Terminal at Valdez every day. The pipeline crosses three active fault traces and was designed to withstand the maximum credible ground shaking and displacements associated with each. One of the intersected faults is the Denali Fault, where the pipeline was designed to accommodate a right-lateral strike-slip displacement of up to 6 m by constructing the supports on horizontal runners. The 3 November 2002  $M_w$  7.9 Denali earthquake ruptured over 300 km of the Denali, Totschunda, and Susitna Glacier faults, including the section beneath the pipeline. The displacement at the pipeline was 5.5 m, and there was only minor damage to some of the supports which had been displaced several meters by the rupture (Sorensen and Meyer, 2003).

Structural control is another relatively new approach to reducing the impact of large earthquakes on various structures. The concept is to suppress the response of a building by either changing its vibration characteristics (stiffness and damping) or applying a control force. There are active, semiactive, and passive types of structural control. Active control systems are defined as those

that use an external power source. The active mass damper is one such device where an auxiliary mass is driven by actuators to suppress the swaying of a building. Kajima Corporation applied this technique to its first building in 1989, and the device is capable of suppressing the response of the building to strong winds and small to medium earthquakes. The high power demand limits its effectiveness for large earthquakes. Passive systems rely on the viscoelastic, hysteretic, or other natural properties of material to reduce or dampen vibrations. Base isolation is one example of a passive system in which large rubber pads separate a building from the ground. These pads shear during strong shaking, reducing the coupling between the building and the ground. These devices have the advantage that they require no external power, little or no maintenance, and perform well in large earthquakes. There are now over 200 buildings around the world with base isolation systems. Finally, semiactive systems use a combination of the two approaches in that the building response is actively controlled but using a series of passive devices. Active variable stiffness and active variable damping devices are currently being used as part of semiactive systems. These semiactive systems have been installed in a few buildings in Japan as they are still in the development mode, but, as with PBSD, they hold the promise of reducing not only the number of fatalities, but also the economic losses associated with future earthquakes.

#### 4.21.4.2 The Implementation Gap

There are two implementation gaps that seriously negate the effectiveness of earthquake-resilient building design. The first is the large variability in their application or enforcement in different countries; the second is that building codes are generally only applicable to new construction.

##### 4.21.4.2.1 *The rich and the poor*

Earthquake-resistant design has been proven effective and building codes that include earthquake provisions have been adopted in most countries that have experienced multiple deadly earthquakes (Bilham, 2004). However, while the number of earthquake fatalities in rich countries is estimated to have decreased by a factor of 10, presumably due to better buildings and land use (Tucker, 2004), the number of fatalities in poor countries is projected to increase by a factor of 10. The 1950  $M$  8.6 Assam earthquake in

India killed 1500 people, but it is estimated that a repeat event in the same location would kill 45 000 people (Wyss, 2004), an increase by a factor of 30 in a region where the population has increased by a factor of 3. Similarly, a repeat of the 1987 M 8.3 Shillong earthquake would kill an estimated 60 times as many people as in 1987 (Wyss, 2004). During that period the population has increased by a factor of 8, again suggesting an order of magnitude increase in the lethality of earthquakes. This increase is largely due to the replacement of single-story bamboo homes with multi-story, poorly constructed, concrete frame structures, often on steep slopes (Tucker, 2004).

Berberian (1990) investigates the earthquake history in Iran. He concludes that the adoption of building codes has had little or no effect, largely due to lack of enforcement. The enforcement gap was also identified after the 1999 Izmit earthquake in Turkey as a major contributor to the 20 000 fatalities. Better implementation and enforcement therefore remain a priority in many earthquake prone regions. However, the socioeconomic situation in many of these countries leaves earthquake risk reduction low on the priority list of development agencies. Most aid organizations continue to operate in a response mode to natural disasters rather than a preventative one. One notable exception is GeoHazards International (<http://www.geohaz.org>), who are working to introduce earthquake-resistant building practices to local builders in regions of high seismic risk.

#### 4.21.4.2.2 *The new and the old*

Building codes only apply to new construction. As is clear from the history of earthquake-resistant building design, every major earthquake to date has provided lessons in how not to construct buildings. Unreinforced masonry was banned for public schools in California after the 1933 Long Beach earthquake. In the most recent earthquakes, problems with moment frame buildings and the dangers of soft story buildings were identified. After each of these earthquakes, building codes are updated. The vast majority of buildings are therefore not up to current code. Several hundred billion dollars are spent every year on construction in seismically hazardous areas of the US. It is estimated that the additional earthquake-related requirements of building codes account for ~1% of this investment; the cost of making new buildings seismically safe is therefore small (Office of Technology Assessment, 1995). In contrast, the

cost of retrofitting existing buildings is much higher, around 20% of the value of the building for most construction types. In addition to the cost, buildings usually need to be vacated during the retrofit causing additional disruption to the occupants. One example of the retrofitting gap comes from a 2001 study of hospital seismic safety in California (Office of Statewide Health Planning and Development, 2001). The study estimated that over a third of the state's hospitals were vulnerable to collapse in a strong ( $6.0 < M < 6.9$ ) earthquake. In Los Angeles County more than half were vulnerable, and the ratio rises to two in three in San Francisco. The total cost of initial improvements required by state law after the 1994 Northridge earthquake totaled \$12 billion; in Los Angeles County, the bill was greater than the total assessed values of all hospital property. Hospitals are considered critical infrastructure, which is why they are required to retrofit by law, but given these economic realities the extent of the retrofits remains to be seen.

The high cost and inconvenience of retrofitting, combined with the uncertainty in the benefit, means that few buildings are retrofitted. However, some institutions and governmental bodies have risen to the challenge. One example of an institution stepping forward to tackle this problem is UC Berkeley (Comerio *et al.*, 2006). The university campus sits astride the Hayward Fault, considered to be one of the most hazardous faults in the SFBA. Since the university was founded, it has had a commitment to the safety of its students, faculty, and staff, and seismic resistant designs have been used across campus. Following the 1971 San Fernando earthquake which caused some damage to another University of California (UC) campus, weaknesses in current building practices were identified and the Universal Building Code was updated in 1976. In 1978, the UC system adopted a seismic safety policy and undertook a review of buildings across the Berkeley campus. Key buildings including University Hall, which housed the system-wide administration at the time, high-rise residence halls, and some key classroom buildings and libraries were retrofitted.

The 1989 Loma Prieta, 1994 Northridge, and 1995 Kobe earthquakes demonstrated how relatively modern buildings were still susceptible to damage during earthquakes and refocused the university on seismic safety. A complete review of campus buildings was ordered in 1996, and it was determined that one-third of all space on campus was rated as poor or very poor, that is, susceptible to collapse in an

earthquake. In 1997, the SAFER program was initiated to retrofit or replace seismically hazardous buildings across campus for life safety. The financial commitment was \$20 million per year for 20 years. The most hazardous buildings were retrofitted first and the program continues today. At the same time that the SAFER program was being formulated, Mary Comerio conducted a study of the broader social and economic impacts of future earthquakes. One of the conclusions was that the campus would likely have to close for one or more semesters after an earthquake on the Hayward Fault. This posed a long-term threat to the university's existence as many students, faculty, and staff would likely move elsewhere during this period and not return. The seismic retrofit program was therefore expanded to include business continuity as a goal in addition to life safety and incorporated elements of performance-based design.

The City of Berkeley has also shown leadership in developing innovative programs to motivate the seismic retrofitting of buildings. One such program is the transfer tax incentive. On purchasing a home, one-third of the transfer tax payable to the city is available for approved seismic retrofitting of the home. This typically amounts to several thousand dollars each time a home changes hands. While an individual homeowner may not fully retrofit the home, as properties change hands over time the building stock becomes more seismically safe. This program, in concert with other city retrofit incentives, has resulted in over 80% of single-family homes being at least partially retrofitted in the city, and an estimated 35% are fully retrofitted, making Berkeley one of the most improved cities for seismic safety in the Bay Area (Perkins, 2003).

It is even more of a challenge to motivate retrofitting of buildings that are not owner occupied. In a program initiated in 2006, the City of Berkeley is targeting the large number of soft story apartment buildings. Soft story buildings have large openings in walls on the ground floor, which, as recent earthquakes have demonstrated, makes them vulnerable to collapse. The openings most commonly allow access to parking under the building or store fronts. Under the new city ordinance, soft story buildings are first identified on a city list and owners are notified. The owner is then required to notify existing and future tenants of the earthquake hazard and postprominent seismic hazard signs. The owners are also required to have an engineering assessment of the seismic safety of the buildings and make the

information available to the city. The program is designed to provide an incentive for owners to retrofit their buildings. The effectiveness of the program will depend on the extent to which tenants are concerned about seismic safety and whether there are alternative accommodations.

#### 4.21.5 Short-Term Mitigation: Real-Time Earthquake Information

The expansion of regional seismic networks combined with the implementation of digital recording, telemetry, and processing systems provides the basis for rapid earthquake information. This process is often referred to as real-time seismology and involves the collection and analysis of seismic data during and immediately following an earthquake so that the results can be effectively used by the emergency response community and, in some cases, for early warning (Kanamori, 2005). One of the first reported calls for real-time earthquakes information came in 1868 following two damaging earthquakes in SFBA in just 3 years. Following the failure of a 'magnetic indicator' for earthquakes, J. D. Cooper suggested the deployment of mechanical devices around the city to detect approaching ground motion and transmit a warning to the city using telegraph cables (Cooper, 1868). Unfortunately, his system was never implemented.

In California, the first automated notification systems provided earthquake location and magnitude information. They used the Real-Time Picker (RTP) and became operational in the mid-1980s. RTP identified seismic arrivals on single waveforms and estimated the signal duration providing constraints on earthquake location and magnitude (Allen, 1978, 1982). In the early 1990s, the systems were further developed to integrate both short-period and broadband information. The Caltech/USGS Broadcast of Earthquakes (CUBE) (Kanamori *et al.*, 1991) and the Rapid Earthquake Data Integration (REDI) Project (Gee *et al.*, 1996; 2003), in southern and northern California, respectively, provided location and magnitude information to users within minutes via pagers.

In Japan, real-time earthquake information systems have been developed in parallel with those in the US. By the 1960s single seismic stations were already being used to stop trains during earthquakes. After the 1995 Kobe earthquake, the Japanese government initiated a program to significantly increase

the seismic instrumentation across the country with multiple seismic networks. The strong-motion Kyoshin Network (K-Net) has over 1000 stations across the entire country with a constant station spacing of 25 km (Kinoshita, 2003). In addition, most of the ~700 short-period instruments deployed in boreholes (Hi-Net) also have strong-motion instruments at the top and bottom of the borehole (KiK-Net). Finally, a lower-density broadband seismometer network consisting of ~70 instruments with a typical station spacing of 100 km spans the entire country. These networks are operated by the National Research Institute for Earth Science and Disaster Prevention (NIED). All data are telemetered in real-time and is available via the web (<http://www.bosai.go.jp>). The Japan Meteorological Agency (JMA) also operates a seismic network across the country which is used for real-time earthquake information.

#### 4.21.5.1 Ground Shaking Maps: ShakeMap and Beyond

Following the 1994 Northridge earthquake, the TriNet project (Mori *et al.*, 1998; Hauksson *et al.*, 2001) was designed to integrate and expand seismic networks and monitoring in southern California. In both the Northridge and 1989 Loma Prieta earthquakes, strong ground shaking occurred away from the epicenter, and there was a need to go beyond point source information and provide better estimates of the locations of likely damage to the emergency response community. In the 1995 Kobe earthquake, it was many hours until the central government in Tokyo was aware of the full extent of damage to the city of Kobe delaying rescue and recovery efforts (Yamakawa, 1998), again emphasizing the need for rapid automated ground shaking information after major earthquakes.

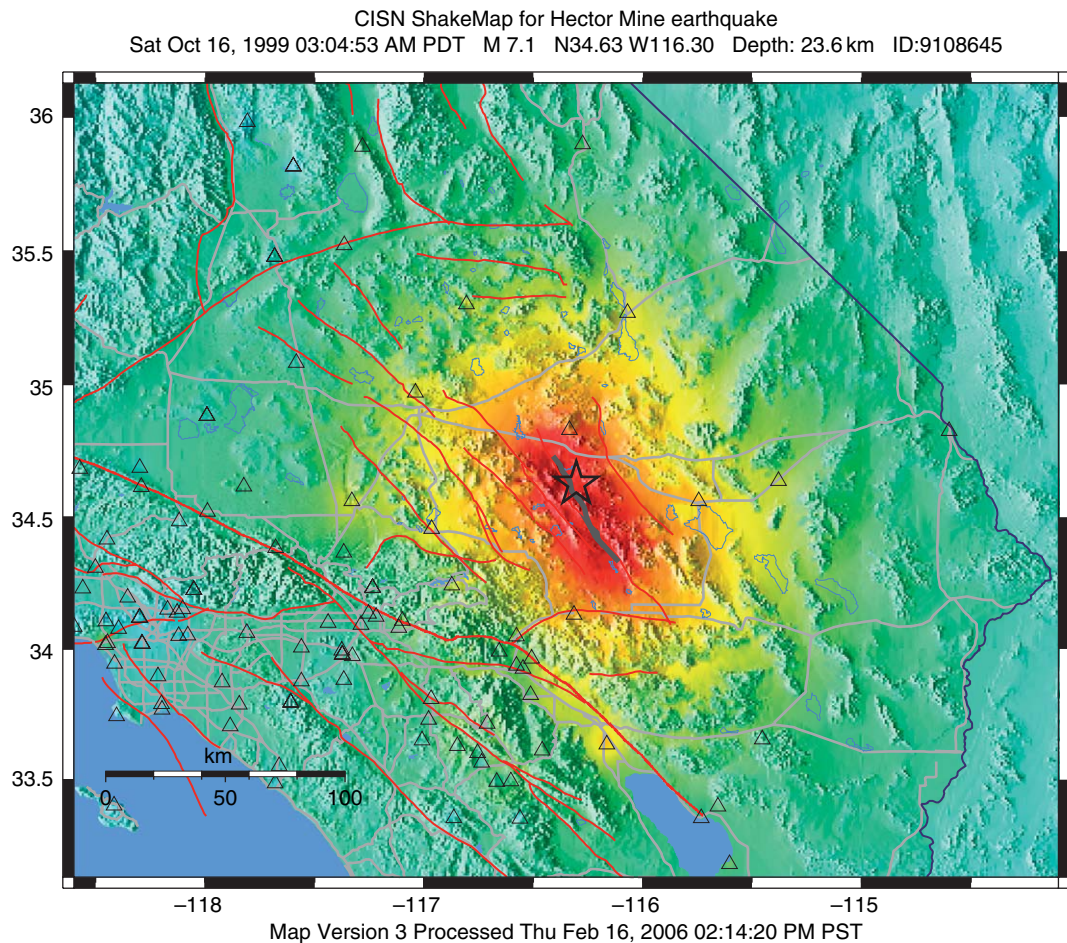
##### 4.21.5.1.1 ShakeMap

The development and implementation of ShakeMap (Wald *et al.*, 1999) was the response of the seismological community. The ShakeMap concept is to rapidly gather ground shaking information following an earthquake and integrate it into a map of peak ground shaking distribution. While the concept is simple, the implementation is complex, as data from different instrument types with a highly heterogeneous distribution must be integrated. The ShakeMap methodology is triggered by the identification of an earthquake, typically with  $M \geq 3$ , and

first gathers PGA and PGV data from seismic instruments in the proximity of the earthquake. The system must wait several minutes for all stations within a few hundred kilometers to record peak ground shaking and telemeter the data to the central processing site.

Once at the central site, individual station data is first corrected for site amplification effects so they represent observations at uniform 'rock' sites. An empirical attenuation relation for an earthquake of the observed magnitude within the region is then adjusted to provide the best-fit relation for the ground shaking as a function of distance. The attenuation relation is used to generate a map of predicted rock-site ground shaking at all locations. This map is adjusted to match local station observations providing a map of ground shaking controlled by the observations close to seismic stations and the best-fit attenuation relation where there are no data. Finally, adjustments are made for site amplification effects based on mapped geology in the region. In addition to providing maps of PGA and PGV, ShakeMap also combines this data and uses scaling relations to provide estimates of instrumental modified Mercalli intensity (MMI) (Wald *et al.*, 1999). MMI was developed prior to modern seismic instrumentation, but still provides a useful description of the felt ground shaking and damage. More detailed information is available in the ShakeMap manual (Wald *et al.*, 2005).

The methodology was in place for the 1999  $M_W$  7.1 Hector Mine earthquake providing a test of the real-time earthquake information system (Hauksson *et al.*, 2003). A location and preliminary local magnitude estimate of 6.6 were first available 90 s after the event origin time. An energy magnitude of 7.0 was available 30 s later. These estimates were broadcast via email, the web, and the CUBE pager system within minutes. The first ShakeMap was produced within 4 min of the event. This initial map was generated using observed peak ground shaking and the best-fit attenuation relation, assuming that the ground shaking decayed as a function of distance from the epicenter. As there was only one station within 25 km of the rupture, near-fault ground shaking was estimated based on the attenuation relations. Over the following hours, ShakeMap was updated using information on the finiteness of the fault based on aftershock locations, finite source inversions, and field observations. Broadband waveforms from more distant sites were used to model the rupture improving the estimates of near-fault shaking



<b>Perceived shaking</b>	Not felt	Weak	Light	Moderate	Strong	Very strong	Severe	Violent	Extreme
<b>Potential damage</b>	None	None	None	Very light	Light	Moderate	Moderate/heavy	Heavy	Very heavy
<b>Peak acc. (%g)</b>	<.17	.17–1.4	1.4–3.9	3.9–9.2	9.2–18	18–34	34–65	65–124	>124
<b>Peak vel. (cm s<sup>-1</sup>)</b>	<0.1	0.1–1.1	1.1–3.4	3.4–8.1	8.1–16	16–31	31–60	60–116	>116
<b>Instrumental intensity</b>	I	II–III	IV	V	VI	VII	VIII	IX	X+

**Figure 10** ShakeMap for the 1999  $M_W$  7.1 Hector Mine earthquake. This version includes the finiteness of the fault rupture which became available in the hours after the earthquake. There is only one seismic station within 25 km of the rupture, so attenuation relations describing MMI as a function of distance from the fault constrain the near-field MMI estimates. The star shows the epicenter and the line represents the finite extent of the fault. The color pallet shows the instrumental MMI.

(Dreger and Kaverina, 2000). The final version is shown in Figure 10.

#### 4.21.5.1.2 Rapid finite source modeling

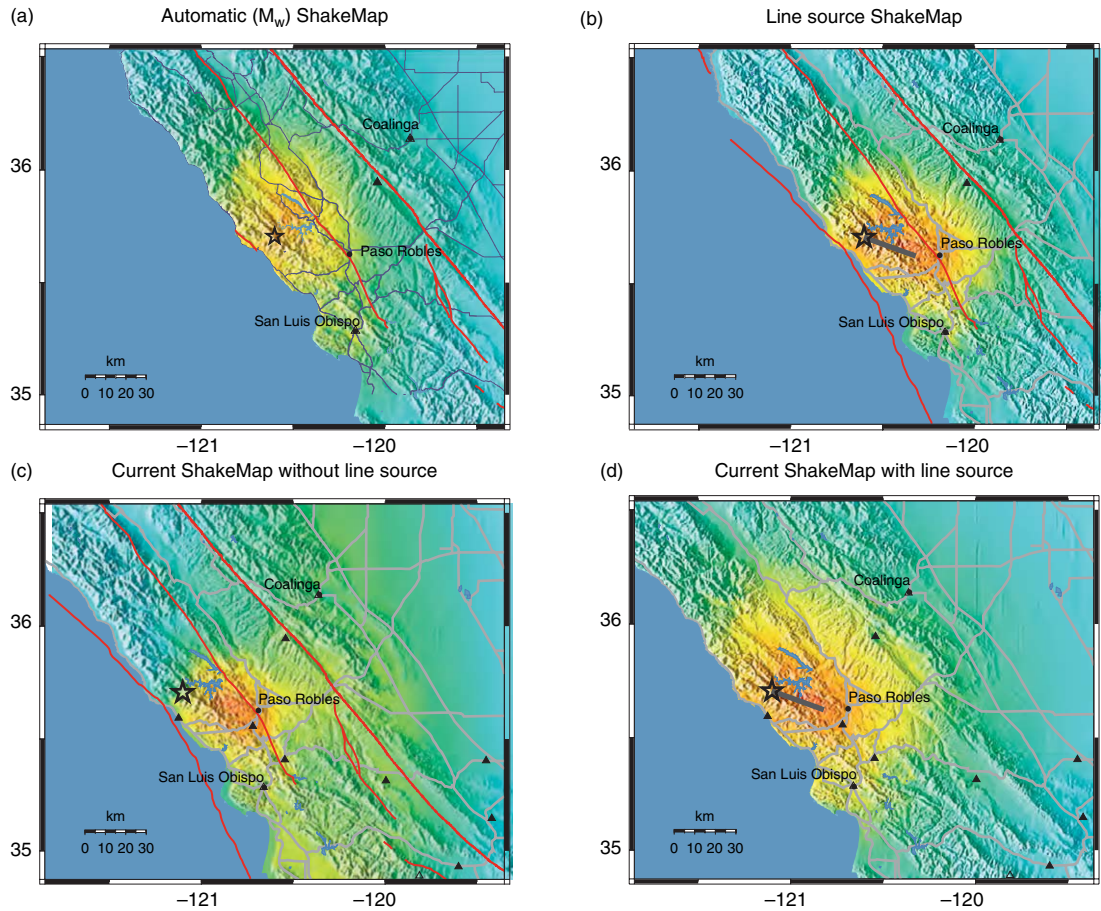
The ShakeMap approach works best in regions with dense station coverage. The observed ground motions then control the contouring of the maps. However, the success of ShakeMap has resulted in a desire to generate maps in regions where the station coverage is sparse to nonexistent. Broadband seismic

stations can be used to model the finiteness of the source and improve the ShakeMap (e.g., Dreger and Kaverina, 2000; Ji *et al.*, 2004). The integration of rapid and automated finite source modeling into ShakeMap-type products represents one of the new directions in seismic hazard mitigation.

The value of finite source information was demonstrated by the 2003  $M_W$  6.5 San Simeon earthquake in central California (Hardebeck *et al.*, 2004; Dreger *et al.*, 2005). The seismic station distribution is

sparse in the region, resulting in only three observations of peak ground shaking close to the event in real time. The initial ShakeMap for the event (Figure 11(a)) is therefore dominated by the event location and magnitude estimate from which

the radial attenuation relation is defined. In fact, the ruptured fault plane extended to the east from the hypocenter, resulting in stronger ground shaking to the east than suggested by this initial ShakeMap. Figure 11(d) shows the best estimate of ground



Perceived shaking	Not felt	Weak	Light	Moderate	Strong	Very strong	Severe	Violent	Extreme
Potential damage	None	None	None	Very light	Light	Moderate	Moderate/heavy	Heavy	Very heavy
Peak acc.(%g)	<.17	.17-1.4	1.4-3.9	3.9-9.2	9.2-18	18-34	34-65	65-124	>124
Peak vel.(cm s <sup>-1</sup> )	<0.1	0.1-1.1	1.1-3.4	3.4-8.1	8.1-16	16-31	31-60	60-116	>116
Instrumental intensity	I	II-III	IV	V	VI	VII	VIII	IX	X+

**Figure 11** ShakeMaps for the 2003  $M_w$  6.5 San Simeon earthquake in central California. Black triangles are seismic stations, the star is the epicenter, and the black line represents the finite extent of the fault. The color pallet shows the instrumental MMI. (a) The automated ShakeMap generated without any finite source information. There are only three stations constraining the ground shaking estimates on the map. (b) The ShakeMap once the length and geometry of the finite source were included based on the information provided by the real-time finite source model. (c) The ShakeMap derived from all available ground motion observation today (including those for which the waveform data had to be transported by hand on magnetic tape) but without any finite source information. (d) The best estimate of the distribution of ground shaking intensity available today. This incorporates the finite extent of the fault and all stations in the region. Modified from Dregler DS, Gee L, Lombard P, Murray MH and Romanowicz B (2005) Rapid finite-source analysis and near-fault strong ground motions; application to the 2003  $M_w$  6.5 San Simeon and 2004  $M_w$  6.0 Parkfield earthquakes. *Seismological Research Letters* 76: 40-48.

shaking available today for comparison; it includes data that were not available in the initial hours after the event.

A real-time finite-source inversion scheme was developed for this scenario by Dreger and Kaverina (2000) using data from the 1992 Landers and 1994 Northridge earthquakes. Although the codes were not automated at the time of 1999 Hector Mine earthquake, they were able to use the offline version to determine finite-source variables and forward calculate ground motions within 5 hours of the event. The now-automated approach (Dreger and Kaverina, 2000) first determines a moment tensor which typically takes 6–9 min. A series of finite-source inversions are then used to explore model space. The moment tensor provides two possible fault planes and the size of the rupture based on moment scaling relations (Somerville *et al.*, 1999). The data are inverted for a series of line sources to test the two moment-tensor nodal planes and a range of rupture velocities. These results are available 11–20 min after the event. At this stage, the orientation and length of the fault plane can be provided to ShakeMap, allowing the ground motion to be estimated as a function of distance from the surface projection of the fault plane rather than distance from the epicenter. A 2-D inversion usually follows, providing a better description of the kinematics of the fault rupture. Finally, the kinematic model can be integrated with near-fault Green's functions to simulate near-fault waveforms, all within ~30 min of an earthquake (Dreger and Kaverina, 2000; Kaverina *et al.*, 2002).

The first event in which the ShakeMap was rapidly updated with finite source information was the 2003 San Simeon earthquake (Dreger *et al.*, 2005). The earthquake occurred in a sparsely populated rural area and most of the damage occurred in the town of Paso Robles 35 km southeast of the rupture where two people were killed. The line-source inversion was complete 8 min after the event and the 2-D inversion and predicted ground motions were available after 30 min. The ShakeMap was updated using the length and geometry of the fault plane derived from the finite source as shown in Figure 11(b). The inclusion of the fault plane resulted in increased estimates of ground shaking at Paso Robles. The initial point-source ShakeMap estimated MMI of V–VI. With the fault plane included in ShakeMap the MMI increased to VII–VIII (compare Figures 11(a) and 11(b)), which is in line with observed damage.

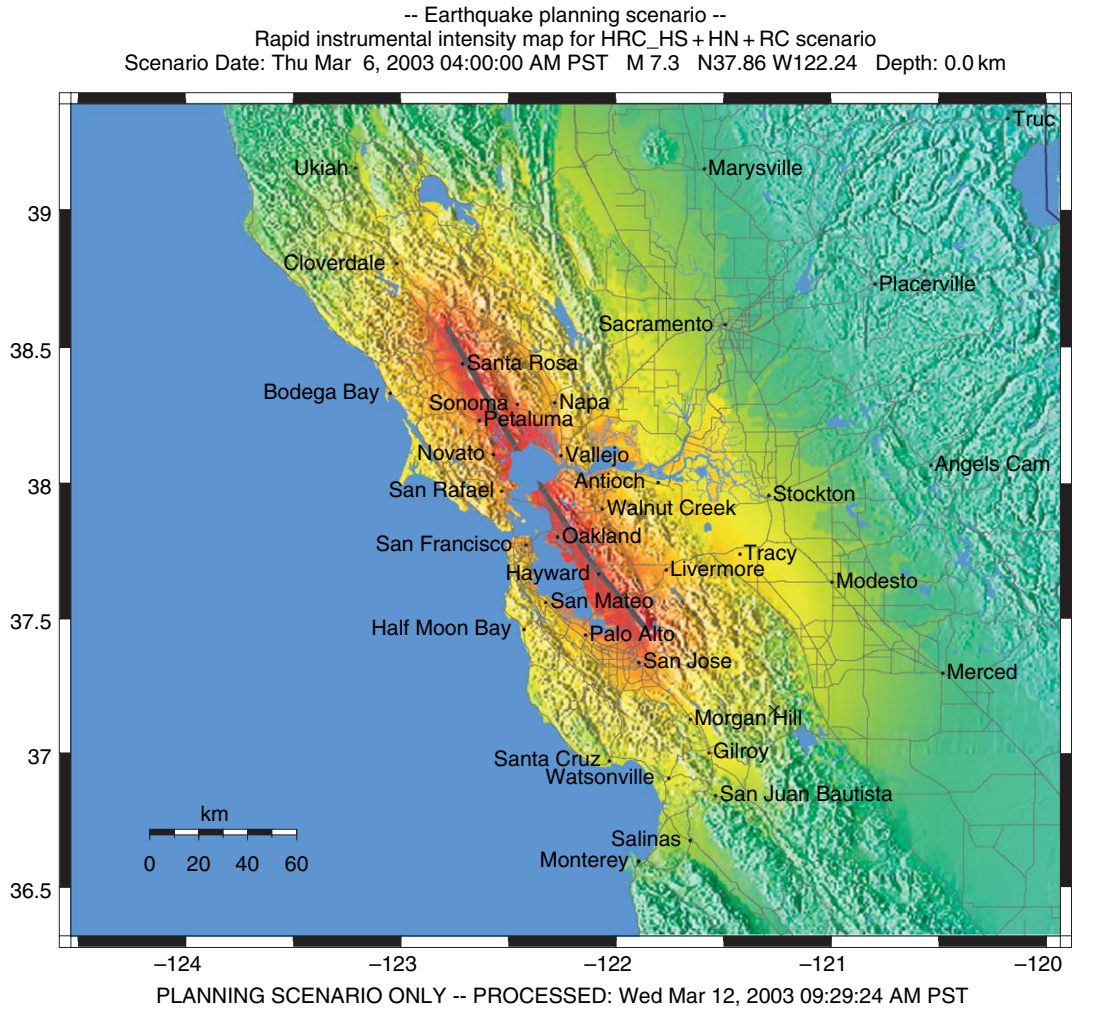
#### 4.21.5.1.3 Applications of ShakeMap

Since its inception, ShakeMap has become a great success, both within the emergency response community for whom it was originally designed, and also with the broader public. While the 1999 Hector Mine earthquake was felt widely across the Los Angeles basin, the ShakeMap showed that the earthquake was fairly distant, centered in the Mohave Desert (Figure 10). This information provided for an appropriately scaled response. One Caltrans bridge crew member reported: “I can't tell you how much time and money was saved knowing where to look [for damage].” ShakeMaps are now routinely generated in Nevada, Utah, the Pacific Northwest, and Alaska in addition to California (visit <http://earthquake.usgs.gov/eqcenter/shakemap/>). Other earthquake-prone regions around the world are also using and developing similar tools. The ShakeMap output also includes GIS shape files of ground shaking levels for use in loss estimation calculations such as HAZUS. These loss estimates are now routinely performed in the hours after moderate and large earthquakes to guide response and recovery.

ShakeMap has also become a tool for public information and education. On the day of the Hector Mine earthquake – ShakeMap's debut – more than 300 000 people visited the website. After smaller, felt earthquakes, website visits reached hundreds per second. In response to this public interest, media maps were designed with the TV audience in mind. These simplified versions of ShakeMap are routinely produced and often used in media coverage following earthquakes. Perhaps the best example of the public interest in the ShakeMap concept is the birth of Community Internet Intensity Maps (CIIMs), better known as “Did you feel it?” These MMI maps are generated automatically using reports of ground shaking intensity provided by the public using an internet portal (<http://earthquake.usgs.gov/eqcenter/dyfi.php>). These reports are averaged by zip code and provide maps that are very similar to the instrumental MMI ShakeMaps. The CIIMs generate thousands of reports after a felt earthquake, the maximum to date was just under 30 000 after an M 5.2 near Anza California in June 2006 (Wald *et al.*, 2006b). In 2004, the USGS extended the CIIM system to allow for international data collection. These ShakeMap-type products have extended the reach and the complexity of earthquake information provided to the public. This provides an inherent educational benefit as the consumers become more informed about earthquake hazards.

The ShakeMap products for the technical user have also been expanding. Maps of the response spectral acceleration at 0.3, 1.0, and 3.0s periods are important for estimating the effects of the shaking on particular types of buildings. This information is also available for past significant earthquakes, prior to the inception of ShakeMap, and thus provides a history of the ground shaking experienced by a particular building. These past

earthquake maps are also useful for planning and training purposes in preparation for future events. Probabilistic assessments of future likely earthquakes, such as those shown for the SFBA above, have also been used to generate scenario ShakeMaps which can be used in loss estimation and also for training. A scenario ShakeMap for a rupture of the Hayward–Rodgers Creek Fault is shown in **Figure 12**. Finally, ShakeCast is a new mechanism



Perceived shaking	Not felt	Weak	Light	Moderate	Strong	Very strong	Severe	Violent	Extreme
Potential damage	None	None	None	Very light	Light	Moderate	Moderate/heavy	Heavy	Very heavy
Peak acc. (%g)	<.17	.17–1.4	1.4–3.9	3.9–9.2	9.2–18	18–34	34–65	65–124	>124
Peak vel. (cm s <sup>-1</sup> )	<0.1	0.1–1.1	1.1–3.4	3.4–8.1	8.1–16	16–31	31–60	60–116	>116
Instrumental intensity	I	II–III	IV	V	VI	VII	VIII	IX	X+

**Figure 12** Scenario ShakeMap for an M 7.3 rupture of the Hayward–Rodgers Creek Fault. This is one of the earthquake rupture scenarios identified by *WG02 (2003)* and was assigned a 1% probability of occurrence by 2032.

for the delivery of ShakeMap which can also be used to trigger user-specific post-earthquake response protocols. For example, utilities, transportation agencies, and other large organizations can automatically determine the shaking at their facilities, set thresholds for notification, and notify responsible staff when appropriate. More information on the range of rapid post-earthquake information products provided by the USGS is available online at <http://earthquake.usgs.gov/>.

#### 4.21.5.1.4 Global earthquake impact: PAGER

All of the rapid post-earthquake information discussed above is seismic hazard information. However, it is the seismic 'risk', that is, the impact of an earthquake, which is more desirable for most consumers. For emergency services personnel, they respond to locations where the greatest hazard intersects the built environment. ShakeCast is intended to provide sophisticated users with the necessary tools to assess the most likely damage to facilities provided the fragility is known. In an ambitious new project, the USGS National Earthquake Information Center (NEIC) is developing a methodology to convert ground shaking hazard into an assessment of impact on the local population. The Prompt Assessment of Global Urban Earthquakes for Response (PAGER) methodology aims to first estimate the distribution of ground shaking and then estimate the number of fatalities (Earle *et al.*, 2005).

To estimate the distribution of ground shaking, that is, a ShakeMap, for a global event the minimum required data are the earthquake location and magnitude, which are routinely determined for global earthquakes with  $M > 5$  by the NEIC. Using available attenuation relations and site corrections derived from the local topography, an initial estimate of the distribution of ground shaking can be made. Additional data that can be input as available include recorded local ground motions, ground shaking intensities reported through the CIIM system, and information about fault finiteness. The finite source information can be derived from a range of sources including aftershock distributions, broadband waveform inversion of teleseismic data (e.g., Ji *et al.*, 2004), and field observation in the hours and days after an event (Wald *et al.*, 2006a). Combining the ShakeMap with population distribution, the number of people experiencing ground shaking at various intensities can be estimated. **Figure 13** shows an example of the PAGER output for the 2005  $M_W$  7.6 Pakistan

earthquake. The methodology estimates that almost 10 million people experienced an MMI of VI, 587 000 experienced MMI IX. Ongoing development of PAGER aims to provide regional fragility information so that these figures can be converted into estimates of the number of casualties.

#### 4.21.5.2 Warnings before the Shaking

The tools and methodologies described above provide rapid post-earthquake information in the minutes to hours after an event. This information is critical to the emergency response community and can prevent cascading failures. It is also useful for longer-term planning and training purposes. But the rapid earthquake information system first described by J. D. Cooper (1868) envisioned a warning system designed to provide an alarm prior to ground shaking. Such warning systems could be used for short-term mitigation in the seconds to tens of seconds prior to ground shaking to prevent damage, casualties, and fatalities. The scientific and engineering challenge for any such warning system is to rapidly distinguish between the frequently occurring small and harmless earthquakes and the large damaging ones.

##### 4.21.5.2.1 S-waves versus P-waves

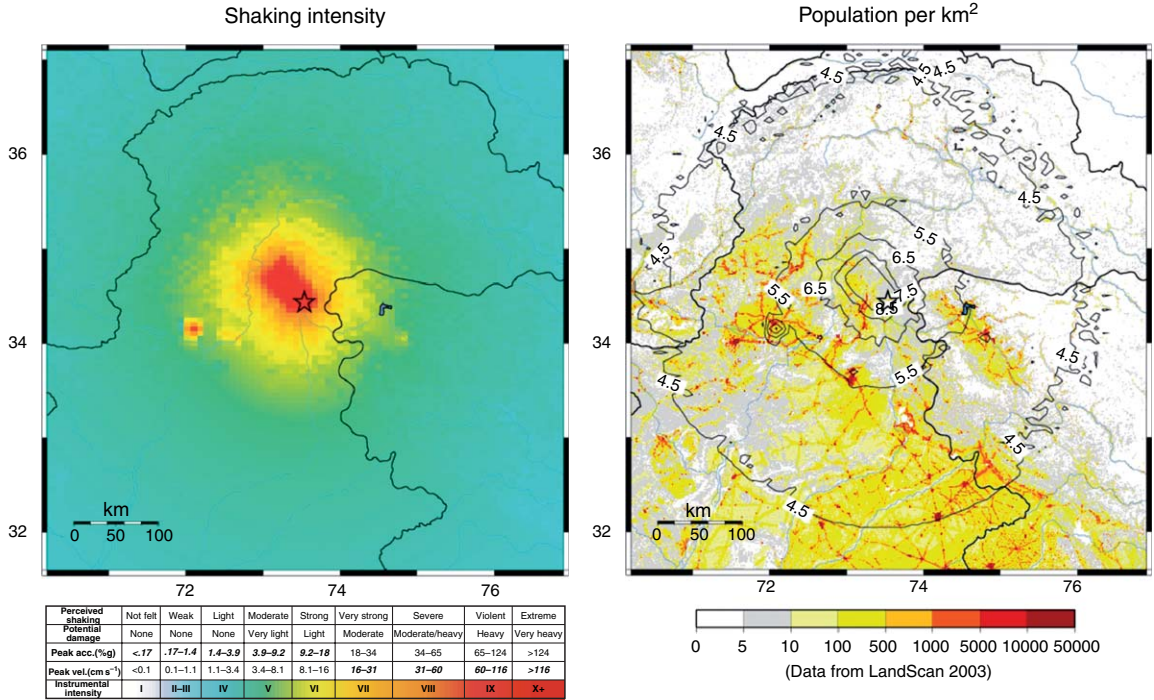
The simplest warning system monitors ground motion and issues an alert or mitigating action when the ground acceleration exceeds some critical threshold. The thresholds are set high, typically  $\sim 0.04g$  (where  $g$  is the acceleration due to gravity), which is the level at which buildings and other infrastructure start to experience permanent damage. These systems therefore trigger on S-wave energy and have a zero warning time but also have the benefit that there is no prediction required; the critical ground shaking has been observed when the alert is issued. Such ground shaking detectors are used widely to shut down utility, transportation, and manufacturing systems during earthquakes.

These detectors can be turned into a true warning system, that is, greater than zero seconds warning, by placing them between the earthquake source and the infrastructure or city they are intended to protect. The warning is then transmitted ahead of ground motion electronically. This 'front-detection' approach is being used in Japan and Mexico, where subduction zone earthquakes along the Japan and Middle America Trenches represent a significant hazard for cities further inland. By deploying stations along the coastline adjacent to the earthquake source

Prompt Assessment of Global earthquakes (PAGER)

M7.6 Pakistan

N34.43 E73.53 10 km sat oct 08, 2005 03:50:38 AM GMT



Population exposed to shaking  
MMI instrumental intensity population

IX	587,000
VIII	1,200,000
VII	1,860,000
VI	9,460,000
V	37,300,000*

**Figure 13** Output from the USGS National Earthquake Information Center's prototype PAGER system. ShakeMap for the event is shown at upper left, and MMI contours are overlain on the population density (upper right). The number of people experiencing different levels of ground shaking can then be tabulated, below. More information is available at <http://earthquake.usgs.gov/eqcenter/pager/>.

region, warning can be transmitted electronically ahead of the ground shaking (Nakamura and Tucker, 1988; Espinosa Aranda *et al.*, 1995). A nonzero warning time requires some form of prediction as ground motion parameters must be detected at one location and estimated for another; this introduces uncertainty. In the case of front detection, ground motion parameters close to the epicenter are used to predict ground shaking levels further away. When the geography is conducive, these systems can provide substantial warning times. In the case of the Seismic Alert System in Mexico, the

~300 km between the subduction zone and Mexico City provide for ~70s of warning as was demonstrated in the 1995 M<sub>W</sub> 7.4 Guerrero earthquake (Anderson *et al.*, 1995).

The amount of warning can be increased by using the P-wave rather than the S-wave energy to assess the magnitude or hazard associated with an earthquake. Nakamura (1988) first proposed such an approach which was implemented along the Shinkansen (bullet train) lines in Japan in the 1990s. Nakamura's approach is to use the predominant period, that is, the frequency content, of the first few

seconds of the P-wave to estimate the magnitude of an earthquake. For seismic stations within  $\sim 150$  km, this measurement is relatively insensitive to epicentral distance and geographical location. Observations from the first few seconds of P-waves recorded within  $\sim 150$  km of the epicenter of  $3 \leq M \leq 8.3$  earthquakes around the world show a scaling relation between magnitude and frequency content,  $\tau_p^{\max}$ , as shown in **Figure 14** (Olson and Allen, 2005). This provides one basis for an early-warning system. The hazard posed by an earthquake is expressed in terms of the magnitude estimate derived from  $\tau_p^{\max}$  of P-waves recorded close to the epicenter. There is uncertainty in magnitude estimates derived from this relation. In the case of the global data set (**Figure 14**) it is  $\pm 1$  magnitude unit, although these uncertainties can be reduced as discussed below. Similar magnitude–frequency scaling relations have been developed for various regions around the world (Allen and Kanamori, 2003; Nakamura, 2004; Kanamori, 2005; Wu and Kanamori, 2005a, 2005b; Lockman and Allen, 2007; Simons *et al.*, 2006), although the approach also has its detractors (e.g. Rydelek and Horiuchi, 2006) (see also Olson and Allen (2006) response).

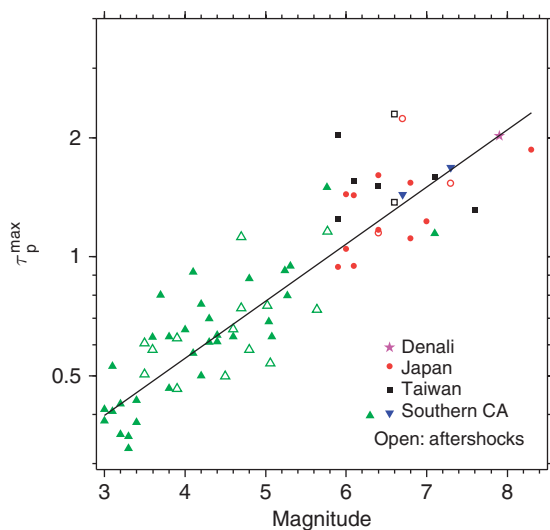


**Figure 14** Scaling relation between earthquake magnitude and the frequency content of the first 4 s of the P-wave recorded at stations within 150 km. This global data set consists of 1842 waveforms recorded from 71 earthquakes. The individual values of  $\tau_p^{\max}$  at each station are averaged on this plot. All the event-averaged values fall within a range of  $\pm 1$  magnitude unit. Modified from Olson E and Allen RM (2005) The deterministic nature of earthquake rupture. *Nature* 438: 212–215.

In addition to using the frequency content of the P-wave, the amplitude can also be used to assess the forthcoming hazard associated with the S- and surface-wave energy. Wu and Kanamori (2005a, 2005b) explored the use of the peak displacement, velocity, and acceleration within the first 3 s of the P-wave. They found that the lower frequency content of the peak displacement has a high correlation with the peak ground displacement (PGD) and the PGV observed many seconds later. **Figure 15** shows the relation between  $P_d$ , the peak ground displacement observed within 3 s of the P-wave arrival, and PGV for 38  $M \geq 5.0$  earthquakes from Taiwan and southern California (Wu *et al.*, in press).  $P_d$  observations at a site can therefore be used to assess the forthcoming ground shaking hazard at the same site.  $P_d$ , and similar amplitude-derived parameters, can also be used to estimate earthquake magnitude once corrected for attenuation associated with the epicentral distance (Odaka *et al.*, 2003; Kamigaichi, 2004; Wu and Kanamori, 2005; Wu and Zhao, 2006; Wurman *et al.*, in review). In a novel hybrid approach, Cua (2005) uses the amplitude of waveform envelopes to estimate the magnitude of an earthquake. The magnitude determination is derived from the ratio of the peak P-wave displacement and acceleration. Given the different

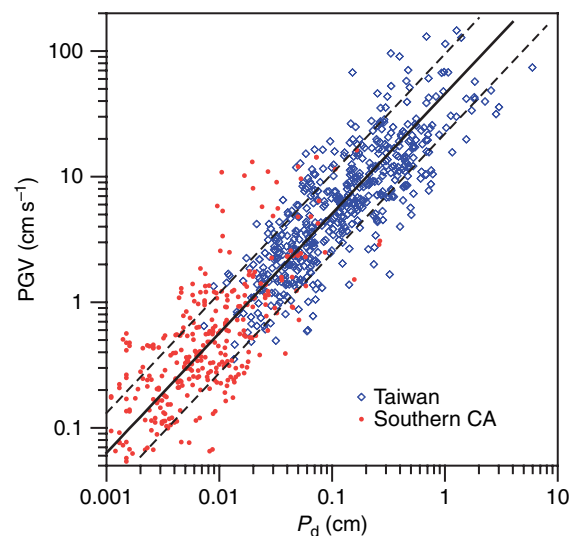


**Figure 15** Scaling relation between  $P_d$  (the peak displacement observed within the first 3 s of the P-wave) and PGV observed at the same station. Data from 38  $M \geq 5.0$  earthquakes in Taiwan (blue) and southern California (red) are shown. Modified from Wu Y-M, Kanamori H, Allen RM, and Hauksson E (in press) Experiment using the tau-c and  $P_d$  method for earthquake early warning in southern California. *Geophysical Journal International*.

frequency sensitivities of the acceleration and displacement waveforms, this approach is analogous to the predominant period approach first suggested by Nakamura, but was arrived at independently using a linear discriminate analysis.

#### 4.21.5.2.2 Single-station and network-based warnings

The simplest and most rapid approach to providing a ground shaking warning is to use a single seismic station to record ground motion parameters and issue a warning on site. The UrEDAS system first outlined by Nakamura (1988) provides an estimate of the magnitude and location of an earthquake using just a single three-component seismometer. Criteria for taking mitigating actions are then developed based on the expected peak ground shaking and warning time which are derived from the magnitude and epicentral distance of the event. Alternatively, rather than first estimating the magnitude, the hazard at the station site can be estimated directly. Figure 15 is an example of this where PGV is estimated directly from  $P_d$ . Combining the amplitude and frequency information from P-waves for  $M \geq 5.0$  earthquakes in Taiwan, Wu and Kanamori (2005) show that the sites that later experienced damaging ground motion could be distinguished from those that did not. The advantage of this approach is its speed. With this approach, it is possible to provide warning at the epicenter. As soon as information about an earthquake is available at a site, action can be taken. The disadvantage, compared to a multiple-station approach, is greater uncertainties in the hazard estimates and the warning time; in some cases, no estimate of the warning time is available. However, choice of appropriate sites for single-station systems can significantly improve their accuracy. Lockman and Allen (2005) applied a similar methodology to UrEDAS to all broadband velocity stations in southern California. They found one quarter of the stations produced magnitude estimates with errors less than  $\pm 0.3$  magnitude units, hypocentral distances within  $\pm 15$  km, and back azimuth calculations within  $\pm 20$  degrees, but the errors at other stations were larger making some unusable for the purpose of early warning.

A network or regional-based approach is the alternative to single-station systems. By combining information from multiple stations, the uncertainties in hazard estimates and the number of false alarms can be reduced. Network-based approaches typically locate an earthquake and estimate its magnitude as a

first step to predicting the expected distribution of ground shaking (Wu and Teng, 2002; Allen and Kanamori, 2003; Kamigaichi, 2004; Cua, 2005; Horiuchi *et al.*, 2005; Allen, in press; Wurman *et al.*, in review). The site-specific peak ground shaking and the time at which it is expected can then be transmitted to users to initiate mitigating actions. When compared with a single-station approach, the cost for users close to the epicenter is a reduced warning time as the system must wait for seismic arrivals at multiple seismic stations and data must be telemetered between sites. However, the introduction of a regional telemetry system increases warning times for users further from the epicenter. For an earthquake detected close to the epicenter, the warning can be transmitted ahead of the ground shaking. This is the front-detection approach described above.

#### 4.21.5.2.3 Warning around the world

It is clear that the most accurate and timely, that is, the most effective, warning systems will combine all of the above approaches making use of information contained in the full waveform and issuing warnings on site as well as taking advantage of a network and telemetry system. Figure 16 shows the locations of the warning systems now in operation and development around the world. Most make use of hybrid methodologies.

The operational systems are in Japan, Taiwan, Mexico, and Turkey, where warnings are issued to users beyond the seismological community. In Japan, the first alarm seismometers were deployed by Japan Railways in the mid-1960s (Nakamura and Tucker, 1988); these detectors were then developed into the more sophisticated UrEDAS P-wave detection system (Nakamura, 1988) in the early 1990s. Since then, network-based approaches have been developed by both the JMA (Kamigaichi, 2004) and the NIED (Horiuchi *et al.*, 2005). JMA has been testing an early-warning system for general use since February 2004 (Kamigaichi, 2004). In August 2006, they widened the testing to 41 institutions, including railway companies, construction firms, factories, and hospitals. As the public becomes more familiar with the system, they plan to make the information more widely available.

The Central Weather Bureau in Taiwan has been using a virtual subnet approach to rapidly assess magnitude from the S-wave energy of an event. This method requires an average of 22 s for magnitude determination and gives warning to populations

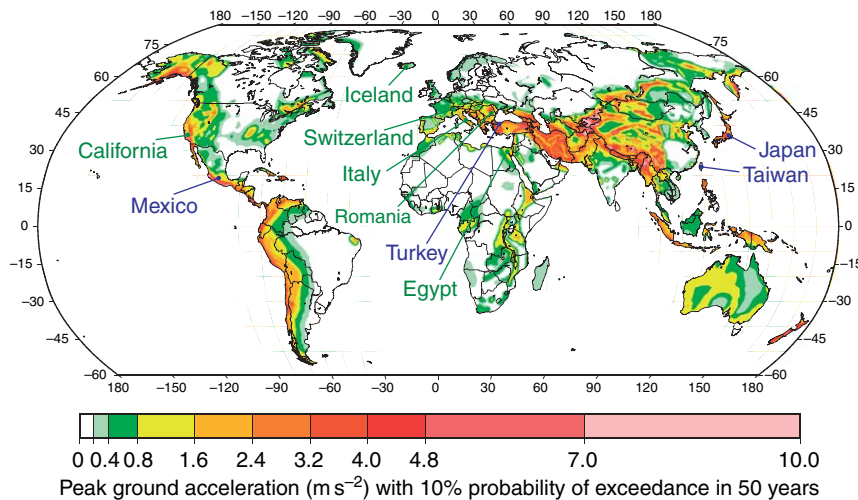


**Figure 16** Map showing the locations of earthquake early-warning systems currently in operation (blue) or development (green) around the world. Operational systems include Japan, Taiwan, Mexico, and Turkey. Systems are in development for California, Egypt, Greece, Iceland, Italy, Romania, and Switzerland. An operational system is defined as one that issues warning information to users outside the seismological community. The locations are overlaid on the GSHAP global seismic hazard map (Giardini *et al.*, 1999).

greater than 75 km away (Wu *et al.*, 1998; Wu and Teng, 2002). The development by Wu and colleagues of P-wave methodologies described above is aimed at increasing the warning times and reducing the blind zone where warnings cannot be provided. Using a network approach, it is estimated that the blind zone would be reduced to 20 km (Wu and Kanamori, 2005). Single-station methodologies could provide warnings at smaller epicentral distances (Wu *et al.*, 2006).

Mexico City's Seismic Alert System (SAS) takes advantage of its geographical separation from the seismic source region along Guerrero Gap subduction zone to the southwest. The front-detection system measures the rate of increase of S-wave energy at stations along the coast to estimate magnitude and transmits this information to the population in Mexico City 300 km away (Espinosa-Aranda *et al.*, 1995). It has been operational since 1991 and transmits its warnings to schools, industry, transportation systems, and government agencies. Finally, Turkey is the most recent member of the early-warning club. Their system triggers when the amplitude of ground motion exceeds some threshold at a network of instruments around the Sea of Marma, providing warning to users in Istanbul (Erdik *et al.*, 2003; Boese *et al.*, 2004).

Development of early-warning systems is also underway across Europe and in the United States. The European Community is currently funding the cooperative development and testing of early warning algorithms in Egypt, Greece, Iceland, Italy,

Romania, and Switzerland. In the United States, the California Integrated Seismic Network (CISN) has recently embarked on a project to test various early-warning algorithms to evaluate their performance across the state. The test includes two network-based approaches, the Earthquake Alarm System (ElarmS) and the Virtual Seismologist (Cua, 2005), and a single-station approach, the amplitude and period monitor (Wu and Kanamori, 2005). The goal is to evaluate the real-time performance and strengths of these methodologies in order to develop an optimal hybrid system for the state. In order to get a sense of the capabilities of such a future system, we consider the performance of one of these methodologies, the one most familiar to the author, in more detail.

#### 4.21.5.2.4 ElarmS in California

The Earthquake Alarm System, ElarmS, is a network-based approach to earthquake early warning (Allen and Kanamori, 2003; Allen, 2004; Allen, in press; Wurman *et al.*, in review; <http://www.ElarmS.org>). The methodology uses the first 4 s of the P-wave arrival at stations in the epicentral region to locate earthquakes in progress and estimate their magnitude. An AlertMap is generated, showing the expected distribution of peak ground shaking in terms of PGA, PGV, and MMI. All available data are collected from all stations every second and the AlertMap is updated. Initially, the AlertMap is based on the location and

magnitude estimates only, and an attenuation relation is used to predict ground shaking. As time proceeds, observations of peak ground shaking near the epicenter are incorporated into the estimate of ground shaking at more distant locations. The predictive AlertMap therefore evolves into an observed ShakeMap during the course of an event.

The ElarmS algorithms were developed using calibration datasets for both southern and northern California. Since February 2006, they have been automatically processing all  $M \geq 3.0$  earthquakes in northern California. They are not yet part of the real-time system and are running in an off-line mode. On notification of an earthquake from CISEN, they sleep for 10 min to allow waveform data to populate the archive. They then gather all available data and process it without human interaction to generate a timeseries of AlertMaps. Between February and

September 2006, there were 83 events processed in this fashion. **Figure 17** shows the AlertMap output for one of the largest events during this period, the  $M_L$  4.7 earthquake near Santa Rosa on 2 August 2006 (local time). The time histories of the magnitude, PGA, PGV, and MMI prediction errors are shown in **Figure 18**. This event was near the Rodgers Creek Fault in a similar location to one of the future hazardous scenario events in the region (WG02, 2003).

The initial detection occurs 3 s after the event origin time (**Figure 17(a)**). The event is located (red star) at the station to trigger (grey triangle) and the warning time across the region is estimated (concentric circles). One second later (**Figure 17(b)**), an additional two stations trigger and the event is relocated using the grid search method. The initial magnitude estimate is also available, derived from the first second of data from the first station to trigger.

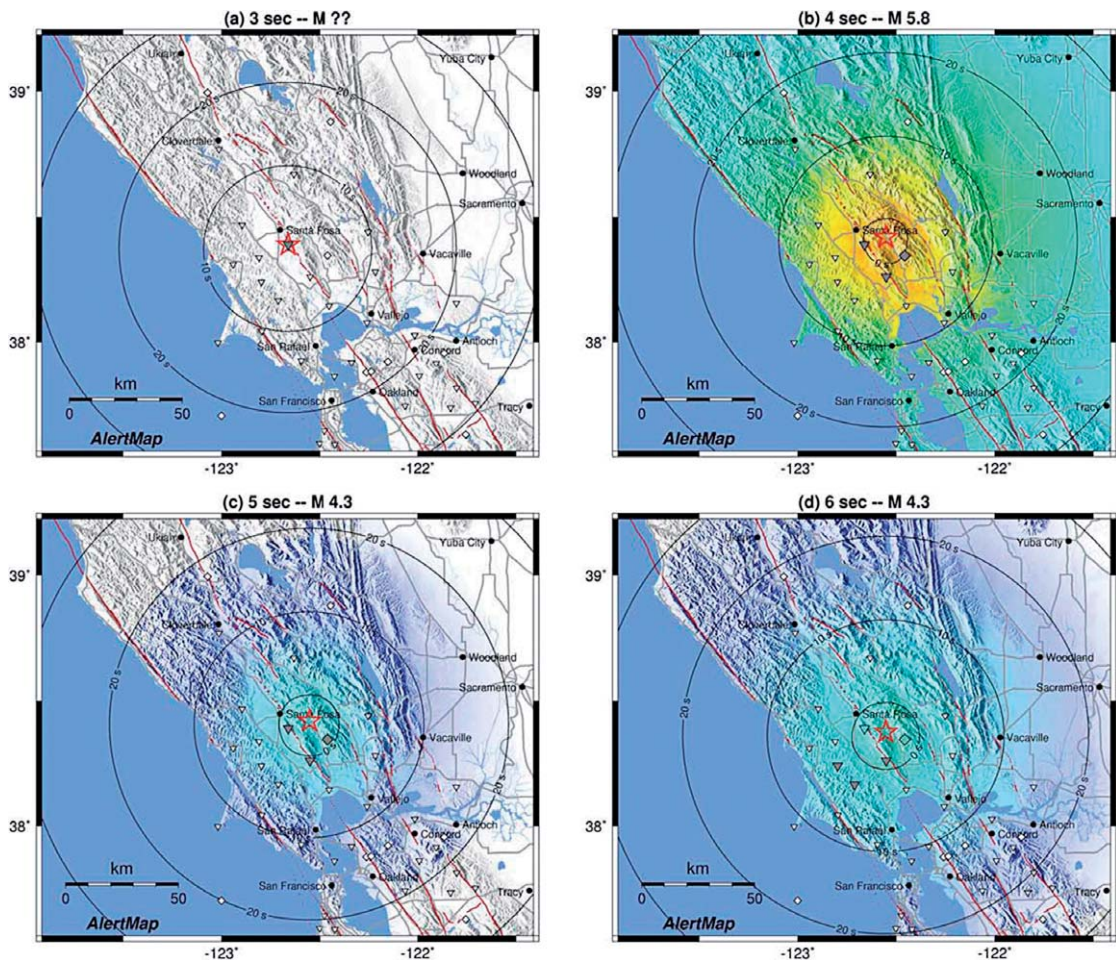
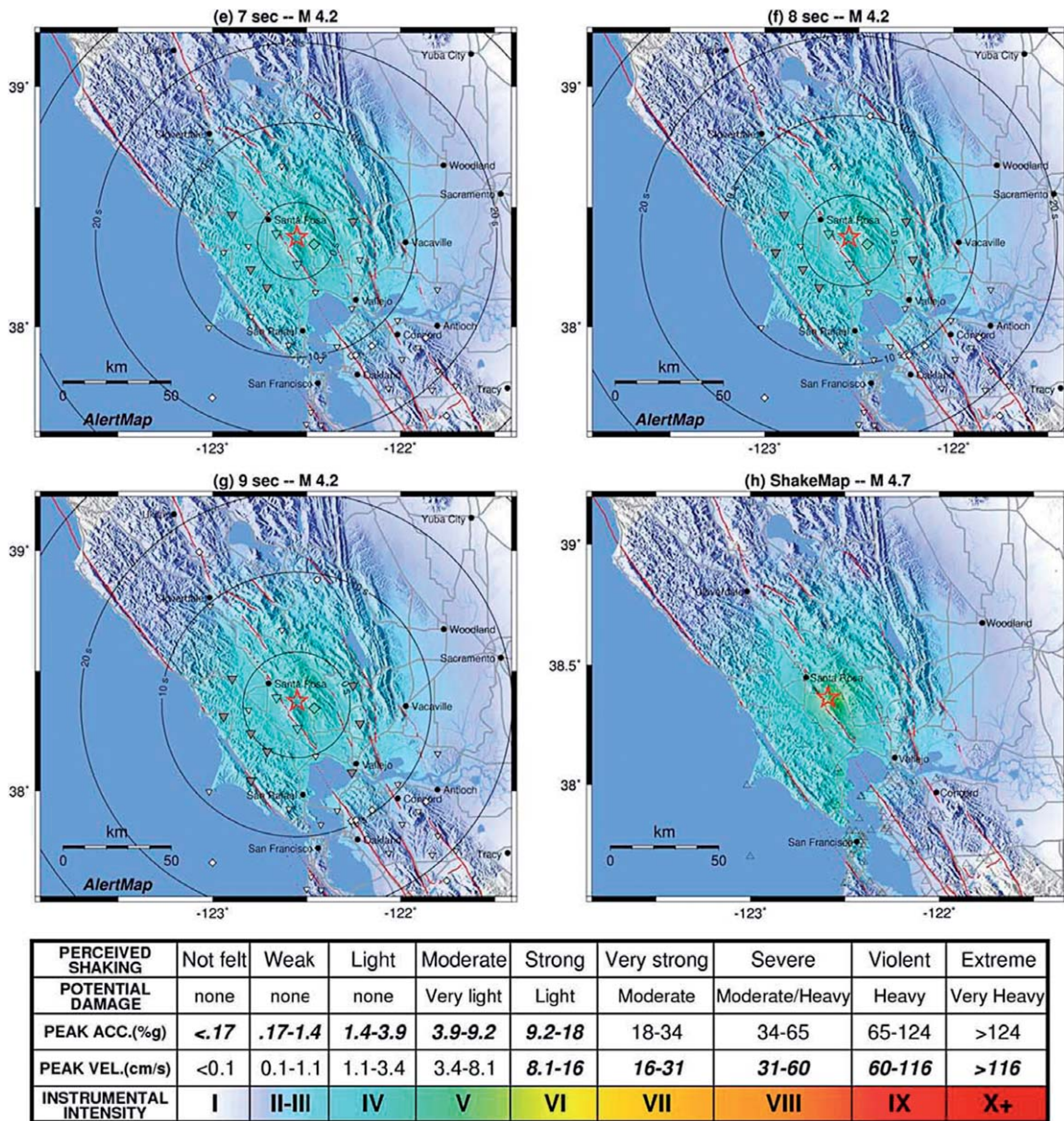


Figure 17 (Continued)



**Figure 17** Performance of ElarmS for the  $M_L$  4.7 earthquake near Santa Rosa on 2 August 2006 (local time). (a–g) AlertMap output from the time of initial detection, 3 s after event origin time, for 8 consecutive seconds. (h) The event Shake Map for comparison. The red star is the event epicenter, concentric circles indicate the warning time. Triangles (broadband velocity), inverted triangles (strong motion), and diamonds (collocated velocity and strong motion) show the locations of seismic station. The symbols turn gray when the station triggers and are colored according to the peak ground shaking at the site once it has occurred. The color pallet shows the predicted instrumental MMI for the AlertMaps (a–g) and the ‘observed’ for the ShakeMap (h).

The initial estimate is high,  $M$  5.8, and the predicted distribution of peak ground shaking is correspondingly high (color pallet). The MMI estimates exceed the actual observations by up to 2 MMI units. One second later (Figure 17(c)), magnitude estimates are available from the additional two triggered stations providing an updated event magnitude estimate of  $M$

4.3. This reduces the predicted MMI intensities and reduces the errors in all output parameters (Figure 18). This illustrates the benefit of using multiple stations. In this case, waiting one additional second so that magnitude information is available from three rather than one stations significantly reduces the error.

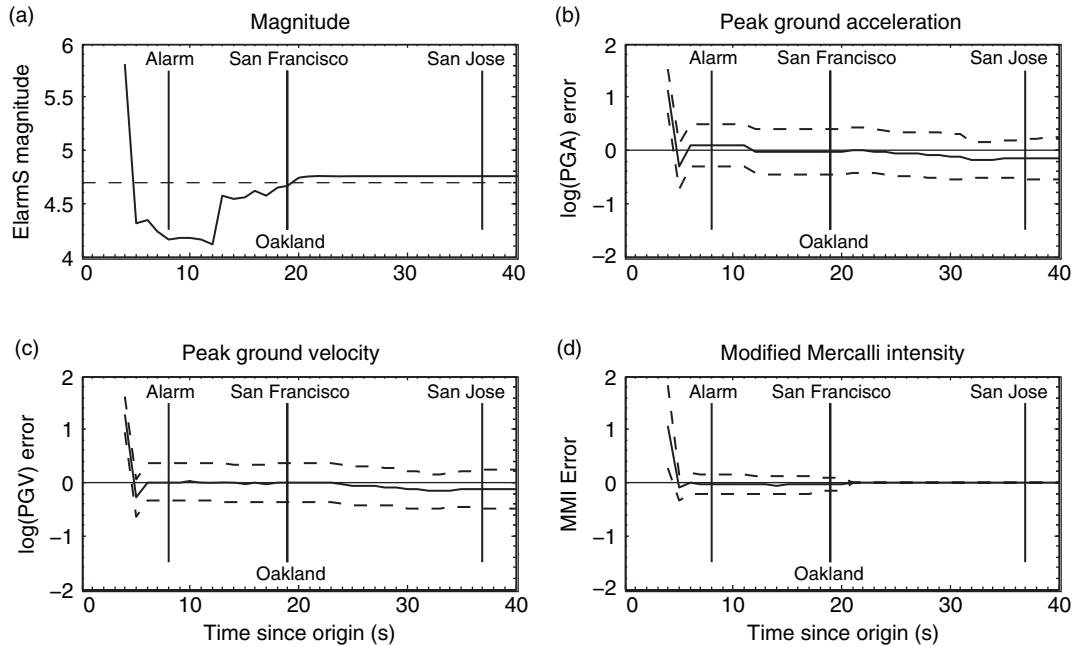


**Figure 18** Performance of ElarmS for the  $M_L$  4.7 earthquake near Santa Rosa on 2 August 2006 (local time) as a function of time. (a) ElarmS magnitude estimate; the dashed line is the CISM magnitude of  $M_L$  4.7. (b) Errors in the predicted PGA determined by subtracting the logarithm of the observed from the logarithm of the predicted. Only stations where the peak ground shaking has not yet been observed are included. The dashed lines represent the one-sigma error envelope. (c) Errors in PGV. (d) Errors in MMI. The MMI error goes to zero, as all stations that have not yet observed peak ground shaking after 20 s had a predicted MMI value of I and an observed value of I. The vertical bars indicate the alarm time (4 sec of P-wave data available from 4 sensors) and the time of peak ground shaking in the cities of San Francisco, Oakland, and San Jose.

One second later, just 3 seconds after the initial detection, peak ground shaking is observed at two stations (Figure 17(d) – colored triangle and diamond), and these observations are used to adjust the attenuation relations for the region. While the magnitude estimate remains 0.4–0.5 units low for the following 6 s (Figure 18(a)), the effect on ground shaking estimates is reduced by the inclusion of these peak ground shaking estimates at the closest stations (Figures 18(b), 18(c), and 18(d)). AlertMaps for the following 3 s are shown in Figures 17(e), 17(f), and 17(g). Additional stations trigger providing information for the magnitude estimate, and peak ground shaking is observed at additional sites, but the predicted distribution of ground shaking does not change noticeably. The CISM ShakeMap for this event is shown in Figure 17(h) for comparison. The AlertMap from 6 s onward is very similar, the main difference being the slightly stronger ground shaking at the epicenter on the ShakeMap. This is due to the underestimates of the ElarmS magnitude which remains low until 13 s, when it reaches  $M$  4.6. Details of the ElarmS methodology and performance in northern California can be found in Wurman *et al.* (in review).

The continuum of information available about an ongoing earthquake is illustrated in Figure 18 which shows the changing error in the predictions. Any individual user can decide whether they would rather react to earlier information which has greater uncertainty but also greater warning time, or wait a few seconds for the uncertainty to reduce. This decision can be made in a probabilistic framework (Grasso, 2005; Iervolino *et al.*, in press; Grasso and Allen, in review). When the cost of inaction in a damaging earthquake and the cost of taking mitigating action are known, the appropriate predicted ground shaking threshold for talking action can be defined provided the uncertainty in the prediction is also known. By only taking action when this threshold is reached, the total cost of an earthquake is minimized.

#### 4.21.5.2.5 Warning times

The maximum warning time for the Santa Rosa event is 15 s for San Francisco and Oakland, and 33 s for San Jose in the south bay. This is the time from the initial magnitude estimation until maximum ground shaking in the cities. However, the initial prediction is high, so it would be preferable to wait

at least a few seconds before taking any actions. The ‘alarm time’ is defined in this chapter as the time at which 4 s of P-wave data are available from four seismic instruments. Application of ElarmS to data sets from southern California, northern California, and Japan shows that the average absolute magnitude error at this time is 0.5 units (Allen, in press; Wurman *et al.*, in review). The alarm time for the Santa Rosa event is shown in **Figure 18**; from alarm time, there is still 11 s warning for Oakland and San Francisco, and 24 s for San Jose. A second  $M_L$  4.7 earthquake occurred in northern California since the automated ElarmS processing began. It occurred on 15 June 2006 near Gilroy south of the bay, and was almost the same distance from San Francisco and Oakland as the 1989 Loma Prieta earthquake. At alarm time for the Gilroy event, when the magnitude estimate was 4.3, there was 3 s of warning for San Jose, 20 s warning for Oakland, and 22 s for San Francisco. In the Loma Prieta earthquake, 84% of the fatalities occurred in Oakland and San Francisco. Therefore, in a repeat of the Loma Prieta earthquake with a warning system in place, there could be  $\sim 20$  s warning in the locations where most casualties occur.

Warning times for earthquakes in California range from zero seconds up to over a minute depending on the location of the earthquake with respect to a population center. Heaton (1985) used a theoretical distribution of earthquakes in southern California to estimate the range of warning times as a function of ground shaking intensities at the warning location. He showed that for the larger, most damaging earthquakes there could be more than 1 min of warning.

Using the ElarmS methodology, we can estimate the warning time for any earthquake location. **Figure 6** contours the warning time the city of San Francisco would have for an earthquake with an epicenter at any location across the region. The warning time is the difference between the alarm time for the earthquake given the current distribution of real-time seismic stations and the time at which peak ground shaking would occur in San Francisco. An additional 5.5 s has been deducted from the warning time to account for telemetry delays of the existing network (which could be reduced).

While **Figure 6** shows the warning time for all earthquake locations, future damaging events will likely occur on specific faults. These likely future damaging earthquake scenarios were identified by WG02. As probabilities are associated with each earthquake scenario, probabilities that an earthquake with a particular warning time will occur by 2032 can be

estimated. **Figure 19** shows that distribution of the warning times for these scenario earthquakes ranges from  $-7$  to 77 s where a negative warning time means the alert time was after the peak ground shaking in San Francisco. The most likely warning times range from  $-7$  to 25 s, which are due to earthquakes on the numerous faults throughout the SFBA (**Figure 6**). The long tail extending to 77 s is due to events on the San Andreas extending to the north. The scenario ShakeMaps for each event (e.g., **Figure 13**) provide an estimate of the ground shaking intensity in San Francisco. The probability distribution shown in **Figure 19** is colored accordingly. The inset to **Figure 19** shows the probability there will be more or less than 0, 5, 10, 20, and 30 s warning and shows that it is more likely that there will be more than 10 sec of warning for the most damaging events. If the telemetry delay was reduced, or more stations were deployed to the north of the SFBA, then more than 20 s warning is likely for these most damaging earthquakes. One of the most deadly scenarios for the city of San Francisco is an  $M$  8, 1906-type earthquake, with a rupture initiating near Cape Mendocino and propagating south. In this scenario, there could be over 1 min of warning time. Probabilistic warning time distributions for various other locations are also available (Allen, 2006).

#### 4.21.5.2.6 Future development

The large-magnitude, most damaging earthquakes are when a warning is of most value and also when the warning times can be the greatest. The accuracy of the ground shaking predictions for these large-magnitude events is significantly improved by knowledge of the finiteness of the rupture. Neither ElarmS, nor any of the other operational early warning systems, currently account for fault finiteness. This is therefore an active area of research. One approach is to monitor the displacement across fault traces allowing instantaneous identification of rupture. This requires instrumentation along all faults and also that the rupture occurs on a previously identified fault at the surface. Some of the earliest proposals for warning systems used wires across fault traces to detect slip. Today, real-time GPS stations could be used to monitor displacement and would be sensitive to slip on fault planes at greater distances. An alternative approach is identifying which seismometers are near-field and which are far-field during the rupture in order to map the rupture extent. Yamada and Heaton (2006) are using the radiated high-frequency energy at near-field stations to approximate the rupture area and the evolving

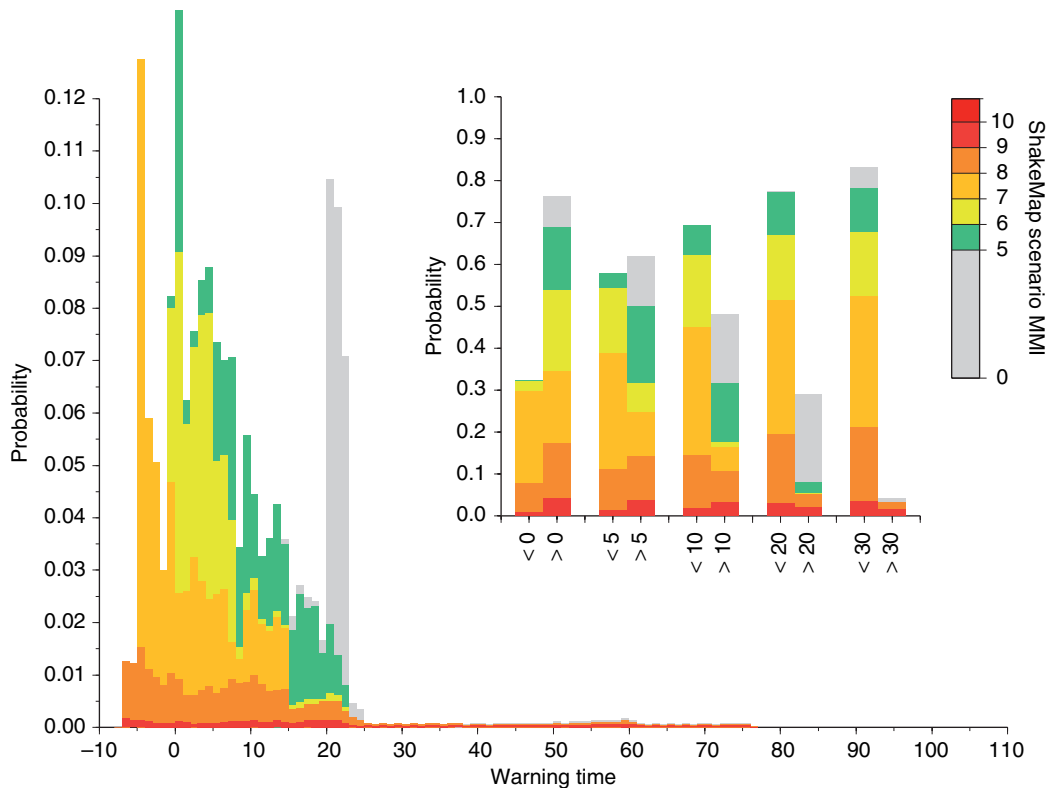


**Figure 19** Warning time probability density function for the city of San Francisco. The warning times for all earthquake scenarios identified by WG02 were estimated given the current seismic network and telemetry delays using ElarmS. The range of warning times is  $-7$  to  $77$  s where a negative warning time means peak ground shaking occurs before the warning is available. The most probable warning times range from  $-7$  to  $25$  s; the long tail extending to  $77$  s is due to the San Andreas Fault. The color shows the predicted intensity of ground shaking in the city. The inset shows the probability of more or less than  $0$ ,  $5$ ,  $10$ ,  $20$ , and  $30$  s warning. It is much more likely there will be greater than zero seconds warning, and the warning times are greater for the most damaging earthquakes. Modified from Allen RM (2006) Probabilistic warning times for earthquake ground shaking in the San Francisco Bay Area. *Seismological Research Letters* 77: 371–376.

moment magnitude in order to estimate the probable rupture length. As these real-time finite-fault techniques are developed, it will be important to incorporate them into early-warning systems.

#### 4.21.5.2.7 Benefits and costs

Warning information from the operational warning systems in Japan, Taiwan, Mexico, and Turkey are currently used by transportation systems such as rail and metro systems, as well as private industries, including construction, manufacturing, and chemical plants. They are also used by utility companies to shut down generation plants and dams, and emergency response personnel to initiate action before ground shaking. In addition, schools receive the warnings allowing children to take cover beneath desks, housing units automatically switch off gas and open doors and windows, and entire complexes

evacuate. These same applications would be appropriate for early-warning implementations in many regions around the world and include both automated response by a computerized control system as well as human response (both for personal protection and reduction of damage to infrastructure).

Looking to the future, earthquake engineering is already evolving to incorporate real-time earthquake information from early-warning systems. In Japan, most new high-rise buildings are ‘dynamic intelligent buildings’ which contain structural control devices to select or change the vibration characteristics of a building, that is, the stiffness or damping (e.g., Housner *et al.*, 1997). Some of these buildings have active control systems which use external power to change or control the building’s response to vibrations. Others have passive devices that use hysteretic or viscoelastic properties of material to reduce

vibrations with no external power. More recently, semiactive systems have been developed which use passive devices that are actively put into operation when necessary. Early-warning information is of value to both the active and semiactive types. As more information about the characteristics of forthcoming ground shaking becomes available (such as amplitude and frequency content), the more effective the building's response systems can be.

For personal protection, early warning systems could perhaps be of most value in regions with high seismic hazard and poor implementation of earthquake-resistant building practices. In many of these underdeveloped environments, buildings are typically small single-story dwellings. Homes may be built by the owner using local materials such as mud bricks. Earthquakes in these regions have high fatality rates as buildings collapse on their occupants. For example, the recent 2003 Bam (Iran) and 2005 Pakistan earthquakes together killed over 100 000 people. In these environments, it only takes a few seconds to get out of these buildings, and early-warning systems could provide that time.

The costs of early-warning systems are substantial, but so are the costs of other mitigation strategies and the earthquakes themselves. California currently has ~300 seismic stations that are telemetered in real-time and appropriate for use in an early warning system. Broad implementation of earthquake early warning in the region would require a more robust and redundant seismic network. To install an additional 600 instruments would cost between \$6 and \$30 million, depending on the instrumentation used. To operate that network would cost between \$2 and \$6 million per year. In addition to these costs, a system to transmit the warning information would be needed as well as an educational program to teach people how to use the information. For comparison, UC Berkeley is currently retrofitting campus buildings to prevent collapse in future earthquakes. The cost per building is typically \$10 to \$30 million; retrofit of the historical Hearst Mining building cost \$80 million and was made possible by a generous donation. UC Berkeley is spending \$20 million per year for 20 years to protect its students and staff in an earthquake, and indeed its very own existence, against a significant earthquake in the region. Implementation of an early-warning system in California is not a replacement for earthquake-resistant buildings and retrofit programs, but there are hundreds of buildings in the SFBA alone like those currently being retrofit on the Berkeley campus

which will not be retrofitted. An early-warning system would allow some short-term mitigation strategies for everyone.

Similarly, in regions where there is little or no implementation of earthquake-resistant building practices, a warning system would provide some mitigation of earthquake effects. The costs could perhaps be reduced by using clusters of stations to improve on single-station performance without requiring a full seismic network. The operation of such systems would have to be done locally, requiring a local seismological skill base. Developing this skill base will also perhaps assist in the improvement of building practices, so both long-term building and short-term warning can be used to reduce the costs of future earthquakes.

#### 4.21.6 Conclusion

Progress in seismic hazard mitigation has been substantial – near-zero fatalities from all earthquakes are within our technical capabilities – and yet the cost of earthquakes is still rising, and the number of fatalities continues to increase.

Reducing the cost and fatalities in future earthquakes requires first identifying the hazard and then implementing appropriate mitigation strategies. Our understanding of the earthquake process allows effective long-term forecasts of hazard expressed as the probability of ground shaking above some threshold. Plate tectonics provides the framework for understanding where most future earthquakes will occur. When considered as a stationary time series, the likelihood of future events can be estimated with a degree of confidence. This provides earthquake probability forecasts on timescales of fifty to hundreds of years. Yet, most in the seismology community would agree that there is a time dependence to earthquake hazard, and the probability of a large earthquake increases with time since the last event as stress increases on a fault. The challenge is to estimate the likely time until the next rupture, which is dependent not only on the rate of increasing stress, but also the initial stress, activity on surrounding faults, and changes in the physical properties of the crust. Given these limitations, the uncertainty in hazard forecasts increases as the forecast timescale decreases.

While the public continues to identify short-term earthquake prediction – the high probability of a clearly defined earthquake in a short period of

time – as the solution to earthquake disasters, few seismologists see such predictions as feasible within the foreseeable future. Existing mitigation strategies, when fully implemented, could reduce the impact of earthquakes more than even the most accurate short-term predictions. This is because predictions would only allow people to get out of the danger area, but the infrastructure on which their lives depend would remain.

Mitigation strategies fall into two categories: long term and short term. Long-term mitigation focuses on building infrastructure capable of withstanding earthquake shaking. This approach has been very effective in reducing the number of fatalities in earthquakes, but still new lessons are learned each time there is a large damaging earthquake. New techniques now allow engineers to test designs against the shaking anticipated from future earthquakes. This provides the opportunity to move beyond the current mode dominated by response to what did not work in the last earthquake. Performance-based seismic design is now also providing a framework for reducing the economic impacts of earthquakes in addition to preventing fatalities.

Short-term mitigation is provided by rapid earthquake information systems. Modern seismic networks have been providing location, magnitude, and ground shaking information in the minutes after an event for over a decade. This information has now been widely integrated into emergency response, allowing for more efficient and effective rescue and recovery efforts. But today, many earthquake-prone regions are pushing the limits of rapid earthquake information systems in an effort to provide similar information in the seconds to tens of seconds before the ground shaking. These warning systems provide another opportunity to further reduce the costs and casualties in future earthquakes.

The reduction of seismic risk will be most effective when multiple approaches are used. There is still a surprise component to all large-magnitude earthquakes, which acts as a reminder that we need to be wary of becoming too tuned in our mitigation efforts. By combining earthquake-resistant design to prevent building collapse, warning systems to isolate toxic systems, and rapid response to critical facilities identified as potentially damaged, we can reduce the impact of an earthquake and also accommodate the failure of one component in the system. In another situation, one mitigation strategy might not be economically feasible while another is. It is therefore

important to continue development of a full range of methodologies.

Perhaps the greatest challenge in seismic hazard mitigation is implementation of these mitigation strategies in all earthquake-prone regions. While the hazard is now clearly identified on a global scale, implementation is extremely variable. All mitigation is local, and the challenge is to provide the necessary resources to the communities that need them. Implementation requires two components: education and incentives. Education about the risk and available mitigation approaches is the first component. But, even when this information is provided, it can be difficult to motivate action for an event that may or may not occur within any individual's lifetime. Incentives are therefore also necessary and can be offered through legal mandate or economic benefit. As the population continues to grow in underdeveloped nations, where cities are increasingly concentrated in earthquake-prone locations and where current mitigation is least effective, the challenge to bridge the implementation gap could not be greater and of more importance.

## Acknowledgments

Gilead Wurman provided several of the figures which were generated with GMT (Wessel and Smith, 1995). Support for this research was provided by USGS/NEHRP Grant # 06HQAG0147.

## References

- Aagaard B (2006) Finite-element simulations of ground motions in the San Francisco Bay Area from large earthquakes on the San Andreas Fault (abstract). *Seismological Research Letters* 77: 275.
- Aki K (1980) Possibilities of seismology in the 1980s. *Bulletin of the Seismological Society of America* 70: 1969–1976.
- Allen CR (1976) Responsibilities in earthquake prediction. *Bulletin of the Seismological Society of America* 66: 2069–2074.
- Allen R (1978) Automatic earthquake recognition and timing from single traces. *BSSA* 68: 1521–1532.
- Allen R (1982) Automatic phase pickers: Their present use and future prospects. *BSSA* 72: S225–S242.
- Allen RM (2004) Rapid magnitude determination for earthquake early warning. In: Pecce M, Manfredi G, and Zollo A (eds.) *The Many Facets of Seismic Risk*, pp. 15–24. Napoli: Università degli Studi di Napoli “Federico II”.
- Allen RM (2006) Probabilistic warning times for earthquake ground shaking in the San Francisco Bay Area. *Seismological Research Letters* 77: 371–376.

- Allen RM (in press) The Elarms earthquake warning methodology and application across California. In: Gasparini P and Zschau J (eds.) *Seismic Early Warning*. Springer.
- Allen RM and Kanamori H (2003) The potential for earthquake early warning in southern California. *Science* 300: 786–789.
- Anderson J, Quaaas R, Singh SK, et al. (1995) The Copala, Guerrero, Mexico earthquake of September 14, 1995 ( $M_w = 7.4$ ): A preliminary report. *Seismological Research Letters* 66: 11–39.
- Bakun WH (1999) Seismic activity of the San Francisco Bay Region. *Bulletin of the Seismological Society of America* 89: 764–784.
- Bakun WH and Lindh AG (1985) The Parkfield, California, earthquake prediction experiment. *Science* 229: 619–624.
- Bakun WH and McEvilly TV (1979) Earthquakes near Parkfield, California: Comparing the 1934 and 1966 sequences. *Science* 205: 1375–1377.
- Berberian M (1990) Natural hazards and the first earthquake catalogue of Iran. Historical hazards in Iran prior to 1900, vol. 1, 649 pp. Tehran: IIEES.
- Bilham R (1988) Earthquakes and urban-growth. *Nature* 336: 625–626.
- Bilham R (1996) Global fatalities from earthquakes in the past 2000 years: Prognosis for the next 30. In: Rundel JB, Turcotte DL, and Klein W (eds.) *Reduction and Predictability of Natural Disasters*, pp. 19–32. Reading, MA: Addison-Wesley.
- Bilham R (1998) Death toll from earthquakes. *Geotimes* 43: 4.
- Bilham R (2004) Urban earthquake fatalities: A Safer world, or worse to come? *Seismological Research Letters* 75: 706–712.
- Boatwright J and Bundock H (2005) Modified Mercalli Intensity Maps for the 1906 San Francisco earthquake plotted in ShakeMap Format, Series. *USGS Open File Report*. 2005–1135.
- Boese M, Erdik M, and Wenzel F (2004) Real-Time prediction of ground motion from P-wave records. *EOS, Transactions of the American Geophysical Union Fall Meeting Supplement* 85: Abstract S21A.0251.
- Boore DM and Zoback MD (1974) Two dimensional kinematic fault modeling of the Pacoima Dam strong motion recordings of February 9, 1971, San Fernando Earthquake. *Bulletin of the Seismological Society of America* 64: 555–570.
- Brocher TM (2005) Compressional and shear wave velocity versus depth in the San Francisco Bay area, California: Rules for USGS Bay Area Velocity Model 05.0.0, Series. *USGS Open-File Report*. 2005–1317.
- Burridge R and Knopoff L (1967) Model and theoretical seismicity. *Bulletin of the Seismological Society of America* 57: 341–371.
- Comerio MC, Tobriner S, and Fehrenkamp A (2006) Bracing Berkeley: A guide to seismic safety on the UC Berkeley campus, Pacific Earthquake Engineering Research Center, Series, PEER 2006/01.
- Cooper JD (1868) Earthquake indicator. *San Francisco Evening Bulletin*, 3 November 1868, p. 10.
- Cornell CA (1968) Engineering seismic risk analysis. *Bulletin of the Seismological Society of America* 58: 1583–1606.
- Cua GB (2005) *Creating the Virtual Seismologist: Developments in Ground Motion Characterization and Seismic Early Warning*. PhD Thesis, Caltech.
- d'Alessio MA, Johanson IA, Burgmann R, Schmidt DA, and Murray MH (2005) Slicing up the San Francisco Bay Area: Block kinematics and fault slip rates from GPS-derived surface velocities. *Journal of Geophysical Research* 110: B06403.
- Dolenc D, Dreger D, and Larsen S (2006) 3D Simulations of ground motions in northern California using the USGS SF06 velocity model (abstract). *Seismological Research Letters* 77: 300.
- Dreger D and Kaverina A (2000) Seismic remote sensing for the earthquake source process and near-source strong shaking: A case study of the October 16, 1999 Hector mine earthquake. *Geophysical Research Letters* 27: 1941–1944.
- Dreger DS, Gee L, Lombard P, Murray MH, and Romanowicz B (2005) Rapid finite-source analysis and near-fault strong ground motions; application to the 2003 Mw 6.5 San Simeon and 2004 Mw 6.0 Parkfield earthquakes. *Seismological Research Letters* 76: 40–48.
- Dunbar PK, Lockridge PA, and Whitewide LS (2006) Catalog of significant earthquakes 2150 B.C. to the present, Series. *NOAA National Geophysical Data Center Report SE-49*. <http://www.ngdc.noaa.gov/nndc/struts/form?t=101650&s=1&d=1> (accessed Jan 2007).
- Earle PS, Wald DJ, and Lastowka LA (2005) PAGER – Rapid assessment and notification of an earthquake's impact, Series, USGS Fact Sheet 2005–2035.
- Erdik MO, Fahjan Y, Ozel O, Alcik H, Aydin M, and Gul M (2003) Istanbul Earthquake Early Warning and Rapid Response System. *EOS, Transactions of the American Geophysical Union Fall Meeting Supplement* 84: Abstract S42B.0153.
- Espinosa-Aranda JM, Jimenez A, Ibarrola G, et al. (1995) Mexico City seismic alert system. *Seismological Research Letters* 66: 42–53.
- Fedotov SA (1965) Regularities of distribution of strong earthquakes in Kamchatka, the Kuril Islands and northern Japan (in Russian). *Akad. Nauk. SSSR Inst. Fiziki Zemli Trudi* 36: 66–93.
- Gee LS, Neuhauser DS, Dreger DS, Pasyanos ME, Uhrhammer RA, and Romanowicz B (1996) Real-time seismology at UC Berkeley: The Rapid Earthquake Data Integration project. *Bulletin of the Seismological Society of America* 86: 936–945.
- Gee L, Neuhauser D, Dreger D, Uhrhammer R, Romanowicz B, and Pasyanos M (2003) The rapid earthquake integration project. In: Lee WHK, Kanamori H, Jennings PC, and Kisslinger C (eds.) *International Handbook of Earthquake & Engineering Seismology*, pp. 1261–1273. San Diego: Academic Press.
- Geller RJ (1996) Debate on evaluation of the VAN method: Editor's introduction. *Geophysical Research Letters* 23: 1291.
- Geller RJ (1997) Earthquake prediction: a critical review. *Geophysical Journal International* 131: 425–450.
- Geller RJ, Jackson DD, Kagan YY, and Mulargia F (1997) Geoscience - Earthquakes cannot be predicted. *Science* 275: 1616.
- Giardini D (1999) The Global Seismic Hazard Assessment Program (GSHAP) - 1992/1999. *Annali Di Geofisica* 42: 957–974.
- Giardini D, Grunthal G, Shedlock KM, and Zhang PZ (1999) The GSHAP Global Seismic Hazard Map. *Annali Di Geofisica* 42: 1225–1230.
- Gokhberg MB, Morgounov VA, and Pokhotelov OA (1995) *Earthquake Prediction: Seismo-Electromagnetic Phenomena*, 193 pp. Singapore: Gordon and Breach Publishers.
- Grasso VF (2005) *Seismic Early Warning Systems: Procedure for Automated Decision Making*. PhD Thesis, Università degli Studi di Napoli Federico II.
- Grasso VF and Allen RM (in review) Uncertainty in real-time earthquake hazard predictions. *Bulletin of the Seismological Society of America*.
- Grunthal G, Bosse C, Sellami S, Mayer-Rosa D, and Giardini D (1999) Compilation of the GSHAP regional seismic hazard for Europe, Africa and the Middle East. *Annali Di Geofisica* 42: 1215–1224.
- Gupta SK and Patwardham AM (1988) Earthquake prediction: Present status, 280 pp. Pune: University of Poona.

- Hanks TC (1975) Strong ground motion of the San Fernando, California earthquake: Ground displacements. *Bulletin of the Seismological Society of America* 65: 193–225.
- Hardebeck JL, Boatwright J, Dreger D, et al. (2004) Preliminary Report on the 22 December 2003, M 6.5 San Simeon, California Earthquake. *Seismological Research Letters* 75: 155–172.
- Harris RA and Simpson RW (1998) Suppression of large earthquakes by stress shadows: A comparison of Coulomb and rate-and-state failure. *Journal of Geophysical Research* 103: 24439–24451.
- Hauksson E, Small P, Hafner K, et al. (2001) Southern California Seismic Network: Caltech/USGS element of TriNet 1997–2001. *Seismological Research Letters* 72: 690–704.
- Hauksson E, Jones LM, and Shakal AF (2003) TriNet: A modern ground-motion seismic network. In: Lee WHK, Kanamori H, Jennings PC, and Kisslinger C (eds.) *International Handbook of Earthquake & Engineering Seismology*, pp. 1276–1284. San Diego: Academic Press.
- Heaton TH (1985) A model for a seismic computerized alert network. *Science* 228: 987–990.
- Horiuchi S, Negishi H, Abe K, Kamimura A, and Fujinawa Y (2005) An automatic processing system for broadcasting earthquake alarms. *Bulletin of the Seismological Society of America* 95: 708–718.
- Housner GW (1984) Historical view of earthquake engineering. *Proceedings of the Eighth World Conference on Earthquake Engineering*, San Francisco, 25–39.
- Housner GW, Bergman LA, Caughey TK, et al. (1997) Structural control: Past, present, and future. *Journal of Engineering Mechanics-Asce* 123: 897–971.
- Housner GW, Martel R, and Alford JL (1953) Spectrum analysis of strong motion earthquakes. *Bulletin of the Seismological Society of America* 42: 97–120.
- Hudson DE (1972) Local distribution of strong earthquake ground motions. *Bulletin of the Seismological Society of America* 62: 1765–1786.
- Iervolino I, Convertito V, Giorgio M, Manfredi G, and Zollo A (in press) Real-time risk analysis for hybrid earthquake early warning systems. *Journal of Earthquake Engineering*.
- Ikeya M (2004) *Earthquakes and Animals*, 295 pp. Singapore: World Scientific Publishing Company.
- Isikara AM and Vogel A (1982) *Multidisciplinary Approach to Earthquake Prediction*, 578 pp. Braunschweig: Friedr. Vieweg & Sohn.
- Jackson DD and Kagan YY (1993) Comment on “Seismic gap hypothesis: Ten years after,” Reply to S.P. Nishenko and L.R. Sykes. *Journal of Geophysical Research* 98: 9917–9920.
- Ji C, Helmberger DV, and Wald DJ (2004) A teleseismic study of the 2002 Denali fault, Alaska, earthquake and implications for rapid strong-motion estimation. *Earthquake Spectra* 20: 617–637.
- Kagan YY and Jackson DD (1991) Seismic gap hypothesis. *Journal of Geophysical Research* 96: 21419–21431.
- Kagan YY and Jackson DD (1995) New seismic gap hypothesis: Five years after. *Journal of Geophysical Research* 100: 3943–3959.
- Kamigaichi O (2004) JMA Earthquake Early Warning. *J. Japan Assoc. Earthquake Eng.* 4.
- Kanamori H (2003) Earthquake prediction: An overview. In: Lee WHK, Kanamori H, Jennings PC, and Kisslinger C (eds.) *International Handbook of Earthquake & Engineering Seismology*, pp. 1205–1216. San Diego: Academic Press.
- Kanamori H (2005) Real-time seismology and earthquake damage mitigation. *Annual Review of Earth and Planetary Sciences* 33: 195–214.
- Kanamori H, Hauksson E, and Heaton T (1991) TERRAScope and CUBE Project at Caltech. *EOS, Transactions, American Geophysical Union* 72: 564.
- Kaverina A, Dreger D, and Price E (2002) The combined inversion of seismic and geodetic data for the source process of the 16 October 1999 M-w 7.1 Hector Mine, California, earthquake. *Bulletin of the Seismological Society of America* 92: 1266–1280.
- Kelleher JA, Sykes LR, and Oliver J (1973) Criteria for prediction of earthquake locations, Pacific and Caribbean. *Journal of Geophysical Research* 78: 2547–2585.
- Kinoshita S (2003) Kyoshin Net (K-Net), Japan. In: Lee WHK, Kanamori H, Jennings PC, and Kisslinger C (eds.) *International Handbook of Earthquake & Engineering Seismology*, pp. 1049–1056. San Diego: Academic Press.
- Kircher CA, Seligson HA, Bouabid J, and Morrow GC (2006) When the big one strikes again – estimated losses due to a repeat of the 1906 San Francisco earthquake. *Earthquake Spectra* 22: S297–S339.
- Knopoff L (1996) Earthquake prediction: The scientific challenge. *Proceedings of the National Academy of Sciences of the United States of America* 93: 3719–3720.
- Kohler M, Magistrale H, and Clayton R (2003) Mantle heterogeneities and the SCEC three-dimensional seismic velocity model version 3. *Bulletin of the Seismological Society of America* 93: 757–774.
- Krishnan S, Ji C, Komatitsch D, and Tromp J (2006) Case studies of damage to tall steel momentframe buildings in southern California during large San Andreas earthquakes. *Bulletin of the Seismological Society of America* 96: 1523–1537.
- Langbein J, Borchardt R, and Dreger D (2005) Preliminary report on the 28 September 2004, M 6.0 Parkfield, California Earthquake. *Seismological Research Letters* 76: 10–26.
- Lawson AC (1908) *The California Earthquake of April 18, 1906*. Washington, DC: Carnegie Institution of Washington.
- Lee WHK, Shin TC, Kuo KW, Chen KC, and Wu CF (2001) CWB Free-Field Strong-Motion Data from the 21 September Chi-Chi, Taiwan, Earthquake. *Bulletin of the Seismological Society of America* 91: 1370–1376.
- Lockman A and Allen RM (2005) Single station earthquake characterization for early warning. *Bulletin of the Seismological Society of America* 95: 2029–2039.
- Lockman A and Allen RM (2007) Magnitude-period scaling relations for Japan and the Pacific Northwest: Implications for earthquake early warning. *Bulletin of the Seismological Society of America* 97: 140–150.
- Lomnitz C (1994) *Fundamentals of Earthquake Prediction*, 326 pp. New York: John Wiley & Sons.
- McCann WR, Nishenko SP, Sykes LR, and Krause J (1979) Seismic gaps and plate tectonics: Seismic potential for major boundaries. *Journal of Pure and Applied Geophysics* 117: 1082–1147.
- McCue K (1999) Seismic hazard mapping in Australia, the southwest Pacific and southeast Asia. *Annali Di Geofisica* 42: 1191–1198.
- McGuire RK (1993) Computation of seismic hazard. *Annali Di Geofisica* 34: 181–200.
- Milne J and Burton WK (1981) *The Great Earthquake in Japan, 1891, 2nd edn., Lane*, 69 pp. Japan: Crawford & Co, Yokohama, and 30 plates.
- Mogi K (1985) *Earthquake Prediction*, 335 pp. London: Academic Press.
- Mori J, Kanamori H, Davis J, and Hauksson E (1998) Major improvements in progress for southern California earthquake monitoring. *EOS* 79: 217–221.

- Nakamura Y (1988) On the urgent earthquake detection and alarm system (UrEDAS). *Proc. 9th World Conf. Earthquake Eng VII*: 673–678.
- Nakamura Y (2004) UrEDAS, Urgent Earthquake Detection and Alarm System, Now and Future. *Proc. 13th World Conf. Earthquake Eng.* August 2004, Paper No. 908.
- Nakamura Y and Tucker BE (1988) Earthquake warning system for Japan Railways' Bullet Trains: Implications for disaster prevention in California. *Earthquakes and Volcanoes* 20: 140–155.
- National Research Council (1971) *The San Fernando Earthquake of February 9, 1971: Lessons from a Moderate Earthquake on the Fringe of a Densely Populated Region*, 24 pp. Washington, DC: National Academy Press.
- National Research Council (2002) *Living on an Active Earth: Perspectives on Earthquake Science*, 418 pp. Washington, DC: National Academies Press.
- National Research Council (2003) *Preventing Earthquake Disasters: The Grand Challenge in Earthquake Engineering*, 172 pp. Washington, DC: National Academy Press.
- Nishenko SP (1989) Earthquakes, hazards and predictions. In: James DE (ed.) *The Encyclopedia of Solid-Earth Geophysics*. New York: Van Nostrand Reinhold 260–268.
- Nishenko SP (1991) Circum-Pacific seismic potential: 1989–1999. *Journal of Pure and Applied Geophysics* 135: 169–259.
- Nishenko SP and Sykes LR (1993) Comment on “Seismic gap hypothesis: Ten years after” by Y.Y. Kagan and D.D. Jackson. *Journal of Geophysical Research* 98: 9909–9916.
- Odaka T, Ashiya K, Tsukada S, Sato S, Ohtake K, and Nozaka D (2003) A new method of quickly estimating epicentral distance and magnitude from a single seismic record. *Bulletin of the Seismological Society of America* 93: 526–532.
- Office of Statewide Health Planning and Development (2001) Summary of hospital performance ratings, Series.
- Office of Technology Assessment (1995) *Reducing Earthquake Losses*. Washington, DC: U.S. Government Printing Office.
- Olsen KB, Day SM, and Minster JB (2006) Strong shaking in Los Angeles expected from southern San Andreas earthquake. *Geophysical Research Letters* 33: L07305.
- Olson E and Allen RM (2005) The deterministic nature of earthquake rupture. *Nature* 438: 212–215.
- Olson EL and Allen RM (2006) Is earthquake rupture deterministic? (Reply). *Nature* 442: E6.
- Olson RS, Podesta B, and Nigg JM (1989) *The Politics of Earthquake Prediction*, 187 pp. Princeton: Princeton University Press.
- Otsuka M (1972) A chain-reaction-type source model as a tool to interpret the magnitude-frequency relation of earthquakes. *Journal of Physics of the Earth* 20: 35–45.
- Perkins J (2003) San Francisco and the Bay Area earthquake nightmare, Series, Association of Bay Area Governments.
- Reid HF (1910) The mechanics of the earthquake, 192 pp. Washington, DC: Carnegie Institution of Washington.
- Rikitake T (1976) *Earthquake Prediction*, 357 pp. Amsterdam: Elsevier.
- Rikitake T (1982) *Earthquake Forecasting and Warning*, 402 pp. Dordrecht: D. Reidel Publishing.
- Rikitake T (1986) *Earthquake Premonitory Phenomena: Database for Earthquake Prediction*, 232 pp. Tokyo: Tokyo University Press.
- Rikitake T and Hamada K (2001) Earthquake prediction. In: Meyers RA (ed.) *Encyclopedia of Physical Science and Technology* 3rd edn., pp. 743–760. San Diego: Academic Press.
- RMS (1995) (Risk Management Solutions, Inc.) What if the 1906 earthquake strikes again? A San Francisco Bay Area scenario, Series, *RMS Report*.
- Romanowicz B (1993) Spatiotemporal patterns in the energy release of great earthquakes. *Science* 260: 1923–1926.
- Rowshandel B (2006) Estimation of future earthquake losses in California. In: Loyd, Mattison, and Wilson (eds.) *Earthquakes of the San Francisco Bay Area and Northern California*. Sacramento: California Geological Survey.
- Rydelek P and Horiuchi S (2006) Is earthquake rupture deterministic? *Nature* 442: E5–E6.
- Shedlock KM and Tanner JG (1999) Seismic hazard map of the western hemisphere. *Annali Di Geofisica* 42: 1199–1214.
- Simons FJ, Dando B, and Allen RM (2007) Automatic detection and rapid determination of earthquake magnitude by wavelet multiscale analysis of the primary arrival. *Earth and Planetary Science Letters* 250: 214–223.
- Sobolev GA (1995) *Fundamentals of Earthquake Prediction*, 161 pp. Moscow: Electromagnetic Research Center.
- Somerville P, Irikura K, Graves RP, Sawada S, and Wald D (1999) Characterizing crustal earthquake slip models for the prediction of strong motion. *Seismological Research Letters* 70: 59–80.
- Song S, Beroza G, and Segall P (2006) A unified source model for the 1906 San Francisco Earthquake (abstract). *Seismological Research Letters* 77: 271.
- Sorensen SP and Meyer KJ (2003) Effect of the Denali Fault rupture on the Trans-Alaska Pipeline. *Proceedings of the 6th U.S. Conference on Lifeline Earthquake Engineering*, Long Beach, CA, August 2003, 1–9.
- Sykes LR, Shaw BE, and Scholz CH (1999) Rethinking earthquake prediction. *Journal of Pure and Applied Geophysics* 155: 207–232.
- Tucker BE (2004) Trends in global urban earthquake risk: A call to the international earth science and earthquake engineering communities. *Seismological Research Letters* 75: 695–700.
- Turcotte DL (1992) *Fractals and Chaos in Geology and Geophysics*, 221 pp. Cambridge: Cambridge University Press.
- Unesco (1984) *Earthquake Prediction*, 995 pp. Tokyo: Terra Scientific Publishing Company.
- United Nations (2004) World urbanization prospects. The 2003 Revision, 185 pp. New York: United Nations.
- Veneziano D, Cornell CA, and O-Hara T (1984) Historical method of seismic hazard analysis, Series, NP-3438.
- Vogel A (1979) *Terrestrial and Space Techniques in Earthquake Prediction Research*, 712 pp. Braunschweig: Friedt. Vieweg & Sohn.
- Wald DJ, Earle PS, Lin K-W, Quitoriano V, and Worden B (2006a) Challenges in Rapid Ground Motion Estimation for the Prompt Assessment of Global Urban Earthquakes, *Proceedings of the 2nd International Workshop on Strong Ground Motion Prediction and Earthquake Tectonics in Urban Areas*, ERI, Tokyo, BERI 8 pp.
- Wald DJ, Quitoriano V, and Dewey JW (2006b) USGS “Did you feel it?” community internet intensity maps: Macroseismic data collection via the internet. *ISEE Proceedings*, Geneva.
- Wald DJ, Quitoriano V, Heaton TH, and Kanamori H (1999a) Relationships between peak ground acceleration, peak ground velocity, and Modified Mercalli Intensity in California. *Earthquake Spectra* 15: 557–564.
- Wald DJ, Quitoriano V, Heaton TH, Kanamori H, Scrivner CW, and Worden CB (1999b) TriNet “ShakeMaps”: Rapid generation of peak ground motion and intensity maps for earthquakes in southern California. *Earthquake Spectra* 15: 537–555.
- Wald DJ, Worden CB, Quitoriano V, and Pankow KL (2005) ShakeMap Manual: Technical Manual, Users Guide, and Software Guide, U.S. Geological Survey, Series, Techniques and Methods 12–A1.

- Wang K, Chen Q-F, Sun S, and Wang A (2006) Predicting the 1975 Haicheng earthquake. *Bulletin of the Seismological Society of America* 96: 757–795.
- Wessel P and Smith WHF (1995) New version of the Generic Mapping Tools released. *Supplement EOS Trans. Amer. Geophys. Union* 76: 329.
- WG02 (2003) Earthquake probabilities in the San Francisco Bay Region: 2002–2031, US Geological Survey, Series, Open File Report 03–214.
- Whittaker A, Moehle J, and Higashino M (1998) Evolution of seismic design practice in Japan. *Structural Design of Tall Buildings* 7: 93–111.
- Wu Y-M and Kanamori H (2005a) Experiment on an Onsite Early Warning Method for the Taiwan Early Warning System. *Bulletin of the Seismological Society of America* 95: 347–353.
- Wu Y-M, Kanamori H, Allen RM, and Hauksson E (in press) Experiment using the tau-c and Pd method for earthquake early warning in southern California. *Geophysical Journal International*.
- Wu Y-M and Teng T-I (2002) A virtual subnetwork approach to earthquake early warning. *Bulletin of the Seismological Society of America* 92: 2008–2018.
- Wu Y-M, Yen H-Y, Zhao L, Huang B-S, and Liang W-T (2006) Magnitude determination using initial P waves: A single-station approach. *Geophysical Research Letters* 33: L05306.
- Wu YM and Kanamori H (2005b) Rapid assessment of damage potential of earthquakes in Taiwan from the beginning of P waves. *Bulletin of the Seismological Society of America* 95: 1181–1185.
- Wu YM, Shin TC, and Tsai YB (1998) Quick and reliable determination of magnitude for seismic early warning. *Bulletin of the Seismological Society of America* 88: 1254–1259.
- Wu YM and Teng TL (2002) A virtual subnetwork approach to earthquake early warning. *Bulletin of the Seismological Society of America* 92: 2008–2018.
- Wu YM and Zhao L (2006) Magnitude estimation using the first three seconds P-wave amplitude in earthquake early warning. *Geophysical Research Letters* 33: L16312.
- Wurman G, Allen RM, and Lombard P (in review). Toward earthquake early warning in northern California. *Journal of Geophysical Research*.
- Wyss M (1979) Earthquake prediction and seismicity patterns (Reprinted from Pure Appl. Geophys., Vol 117, No 6, 1979), 237 pp. Basel: Birkhauser Verlag.
- Wyss M (1991) *Evaluation of Proposed Earthquake Precursors*, 94 pp. Washington DC: Am. Geophys. Un.
- Wyss M (2004) Human losses expected in Himalayan earthquakes. *Natural Hazards* 34: 305–314.
- Yamada M and Heaton T (2006) Early warning systems for large earthquakes: Extending the virtual seismologist to finite ruptures (abstract). *Seismological Research Letters* 77: 313.
- Yamakawa K (1998) The Prime Minister and the earthquake: Emergency management leadership of Prime Minister Marayama on the occasion of the Great Hanshin-Awaji earthquake disaster. *Kansai Univ. Rev. Law and Politics* 19: 13–55.
- Zhang P, Yang Z-X, Gupta HK, Bhatia SC, and Shedlock KM (1999) Global seismic hazard assessment program (GSHAP) in continental Asia. *Annali Di Geofisica* 42: 1167–1190.